Atmospheric blocking types: Frequencies and transitions

Carola Detring[1,2,], Annette Müller[1], Lisa Schielicke[1], Peter Névir[1], and Henning W. Rust[1]

[1]Institut für Meteorologie, Freie Universität Berlin, Germany
[2]Meteorologisches Observatorium Lindenberg - Richard-Aßmann-Observatorium, Deutscher Wetterdienst, Germany

Correspondence: Carola Detring (carola.detring@dwd.de)

Abstract. Stationary, long-lasting blocked weather patterns can lead to extreme conditions such as very high temperatures or heavy rainfall. They are defined by a persistent high pressure system in combination with one or two low pressure systems. The mechanisms for the onset of such weather patterns are still not fully understood. Using a novel method based on the kinematic vorticity number we distinguish between two blocking types, namely *High-over-Low* and *Omega* block, in previously-identified
5   blocking periods. Our main goal of this work is to study the temporal evolution of the occurrence probability and the onset, offset, and transition probabilities of blocking on the northern hemisphere. We analyze NCEP-DOE Reanalysis 2 data over the 30 year period from 1990 to 2019 in two regions: Euro-Atlantic sector (40°W-30°E) and half northern hemisphere (90°W-90°E). First, we use logistic regression to investigate the temporal development of blocking probabilities depending on years, seasons and months. We find no significant difference in blocking numbers over the 30 year period. But we find large differences
10   in the occurrence probabilities on a monthly basis with strongest increases over the 30 year period in February and March that are compensated by a decrease in December and autumn. Second, we use a Markov model to calculate the transition probabilities for two models: One is composed of two states *blocking* and *no blocking*, and another Markov model (three states) that additionally distinguishes between the specific blocking types *High-over-Low* and *Omega* blocking as well as of the state *no blocking*. The description with Markov theory reduces the probability to change from one weather regime to
15   another or to stay within the same regime to a dependency only on the previous time step. Over the 30 year period, we found the largest changes in transition probabilities in the summer season, where the transition probability to *Omega* blocks increase strongly, while the *unblocked* state becomes less probable. Hence, *Omega* blocks become more frequent and stable in summer at the expense of the other states. As a main result, we show that *Omega* blocking is more likely to occur and more persistent than the *High-over-Low* blocking pattern.

20 **1 Introduction**

´ A blocking is a quasi-stationary, persistent large-scale atmospheric flow pattern that blocks the typical westerly flow and forces the jet and embedded pressure systems to bypass on its northern and southern sides (e.g. Rex, 1950). Besides Rex (1950) initial definition of 10 days, typically a minimum blocking duration of 4 to 5 days is assumed (e.g. Pelly and Hoskins, 2003; Barriopedro et al., 2006, 2010; Barnes et al., 2011). Typical block patterns are steady ridges, *High-over-Lows* (dipoles) and
25   *Omega* blocks (tripoles) (see e.g. Bott, 2012; Woollings et al., 2018). The latter two consist of a poleward high accompanied by one or two lows on its equatorward side. Often, a transition between the *High-over-Low* and the *Omega* blocking patterns and
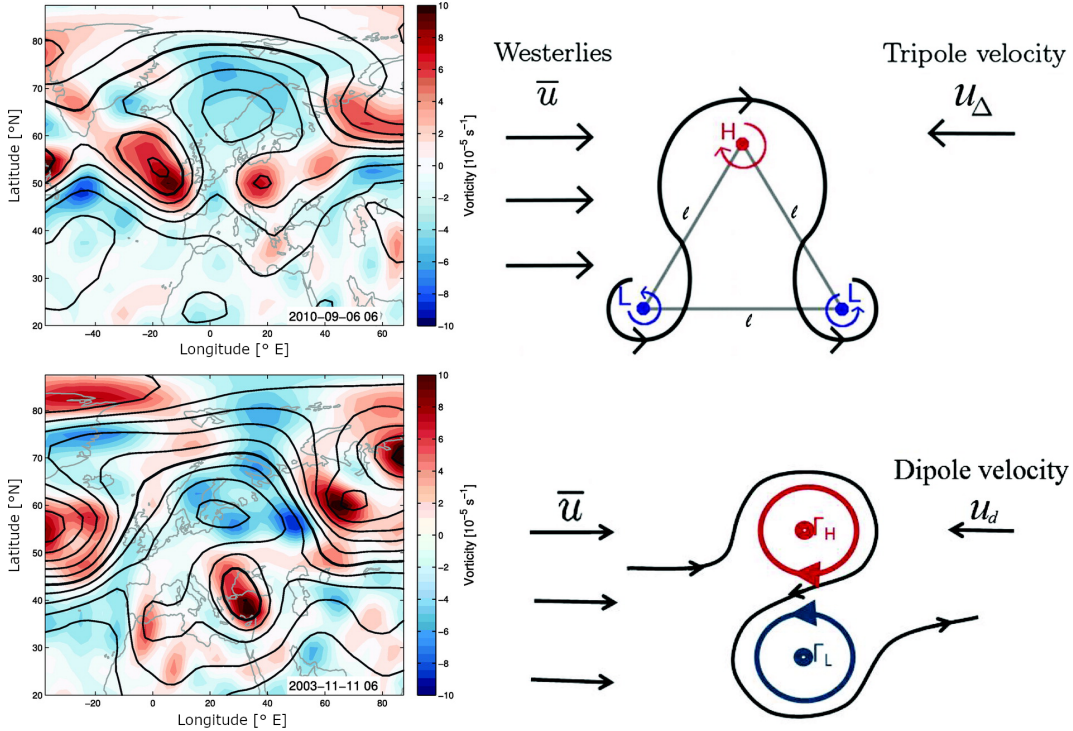
vice versa could be observed. Such a transition is documented in Schielicke (2017, appendix A.3, Fig. A69) for summer 2010, where long-lasting blocking caused extreme heat and forest fires over Russia. Due to its persistence, blocking can determine the weather, especially temperature and precipitation patterns, in the mid-latitudes for several days up to several weeks. Depending
30 on the block's location, duration and intensity, it can have devastating, regional impacts ranging from heatwaves and droughts in the warm season to cold spells in winter and spring (e.g. Pfahl and Wernli, 2012; Brunner et al., 2017, 2018).

  Especially in recent years, heatwaves, droughts and temperature records in the summer season made the headlines. In the past two years, 2018 and 2019, a series of blocking led to exceptional, "unprecedented" drought conditions in the two consecutive summers (Hari et al., 2020). As a result of *Omega* blocking situations that occurred in June and July 2019, widespread
35 temperature records far above 40°C were reported in western and central Europe with an observed record temperature of 45.9°C in southern France at 28 June 2019 (Henley et al., 2019) and 42.6°C in western Germany on 25 July 2019 (Deutscher Wetterdienst, 2019; Bissolli et al., 2019). However, the long lasting high accompanied by one or two persistent low pressure areas can lead to contrary devastating weather situations. For example, the *Omega* blocking that caused the persistent heatwave over Russia in June to August 2010 also led to "record-breaking" floods downstream in Pakistan (e.g. Hong et al., 2011). At the
40 western flank of a quasi-stationary blocking over northern Europe in May/June 2018, an unusual high number of slow-moving thunderstorms caused heavy rain rates and flash floods in large parts of western and central Europe (Mohr et al., 2020).

  A concept of atmospheric blocking based on an idealized point vortex model was introduced by Obukhov et al. (1984), and further studied in Kuhlbrodt and Névir (2000); Müller and Névir (2014); Müller et al. (2015). This model describes the dynamics of vortices under the highly-idealized conditions of a two-dimensional, incompressible, inviscid flow. It is a
45 discretized formulation of the vorticity equation. Mathematically, it is represented by a system of coupled non-linear ordinary differential equations, which goes back to (Helmholtz, 1858). Each point vortex induces a circular, radial-symmetric velocity field around its position, whose orientation and strength depend on the circulation Here, cyclonic rotation is connected to a positive circulation and anticyclonic rotation to a negative circulation. For each vortex, the circulation is conserved. The motion of a set of point vortices is then determined by their circulations and the intervortical distances only. For further physical details
50 of the point vortex theory see e.g. Aref (1979); Newton (2001). Hirt et al. (2018) statistically confirm the theory of Müller et al. (2015) that the *Omega* blocking pattern can be regarded as a three point vortex system (tripole) with the anticyclonic point vortex, i.e. the high, located on the poleward side of two cyclonic point vortices. The three point vortex system "moves" westwards under certain conditions[1] opposing the typical westerly wind of the mid-latitudes, and thus can become stationary if both speeds are identical. Analogously, a *High-over-Low* block can be described by a point vortex pair (dipole) that moves
55 westward. This concept is summarized in Fig. 1 and we will use it to identify and classify blocking types in this paper. It should be noted, that this discrete perspective is contrary to the explanation of the blocking based on Rossby-waves as studied by e.g. Tung and Lindzen (1979). Further authors, Tyrlis and Hoskins (2008), Berrisford et al. (2007), Altenhoff et al. (2008) describe the onset of blockings with the Rossby wave breaking.

---

[1]The sum of the circulations is zero; in case of the *Omega* blocking, the vortices lie on the vertices of a equilateral triangle with the high on the poleward tip.

Figure 1. Application of point vortex theory to two distinct atmospheric blocking types: (top) *Omega* blocking and (bottom) *High-over-Low* blocking. (Left) Two exemplary blocking events observed at the 500 hPa level: Displayed is the vorticity (colour-shaded) and contours of geopotential height in 8 dm intervals (bold contour represents 552 dm). (Right) Illustration how the corresponding blocking can be realized in the point vortex model. Figure is adapted from Hirt et al. (2018, their figure 2, published under the terms of the Creative Commons Attribution License (http://creativecommons.org/licenses/by/4.0/)) with upper right figure taken from Müller et al. (2015). The point vortex systems become stationary if the westerlies dipole/tripole velocities are of equal magnitude.

Blocking identification depends on the specific definition used; therefore, blocking climatologies can differ with respect to

60 frequency and location of blocking (e.g. Barriopedro et al., 2010). Although different methods yield different results, they agree in two general aspects: blocking maxima are observed in the North Pacific and North Atlantic-European region, and higher blocking numbers occur in boreal winter compared to the summer season (e.g. Pinheiro et al., 2019). However, larger variability is observed on a block-to-block basis (Pinheiro et al., 2019) and from year-to-year (Davini et al., 2012).

The numerical prediction of blocking onset and persistence, i.e. the transition from zonal to blocked flow and vice versa,

65 is still a challenge. Ferranti et al. (2015) showed that medium-range ensemble forecasts in the Euro-Atlantic region are less skillful in these situations. Transitions between different large-scale weather regimes have been studied by cluster analyses and the application of Markov chains by e.g. Spekat et al. (1983); Egger (1987); Vautard et al. (1990); Kimoto and Ghil (1993). A Markov model describes the probabilities of transitions between the states of a system. For this purpose, only the present state is taken into account. Hence, the future state becomes independent of all previous states except of the current one (e.g.

70 Grewal et al., 2019). Spekat et al. (1983) (as described in Egger, 1987) differentiate between three discrete states of central European large-scale weather regimes, also called *Grosswetterlagen*: zonal, meridional and mixed state (see e.g. Werner and Gerstengarbe, 2010). While zonal *Grosswetterlagen* are characterized by west winds only, meridional regimes are determined by blocking highs, but also by trough patterns. Finally, mixed states are characterized by mixed flow situations such as south- or northwesterly flow. Spekat et al. (1983) found relatively long residence times within the states of 5 to 7 days and relatively

75 low probabilities of 5 % to 11 % for the transition between the three states on a day-to-day basis. However to our knowledge, the transition between different blocking types, i.e. *Omega* and *High-over-Low* blocks, and the non-blocked state has not been studied so far on a sub-daily, 6-hourly time scale.

The question arises, if one can examine the transition and occurrence probabilities of atmospheric blocking in an event-based, sub-daily manner? Are there trends in the general blocking situation or in the blocking types? Is there a seasonal dependence for

80 the different blocking types? In order to tackle these open questions, we will estimate the transition probabilities of occurrence of *High-over-Low*, *Omega* blocking, and *non-blocked* states in terms of a Markov process.
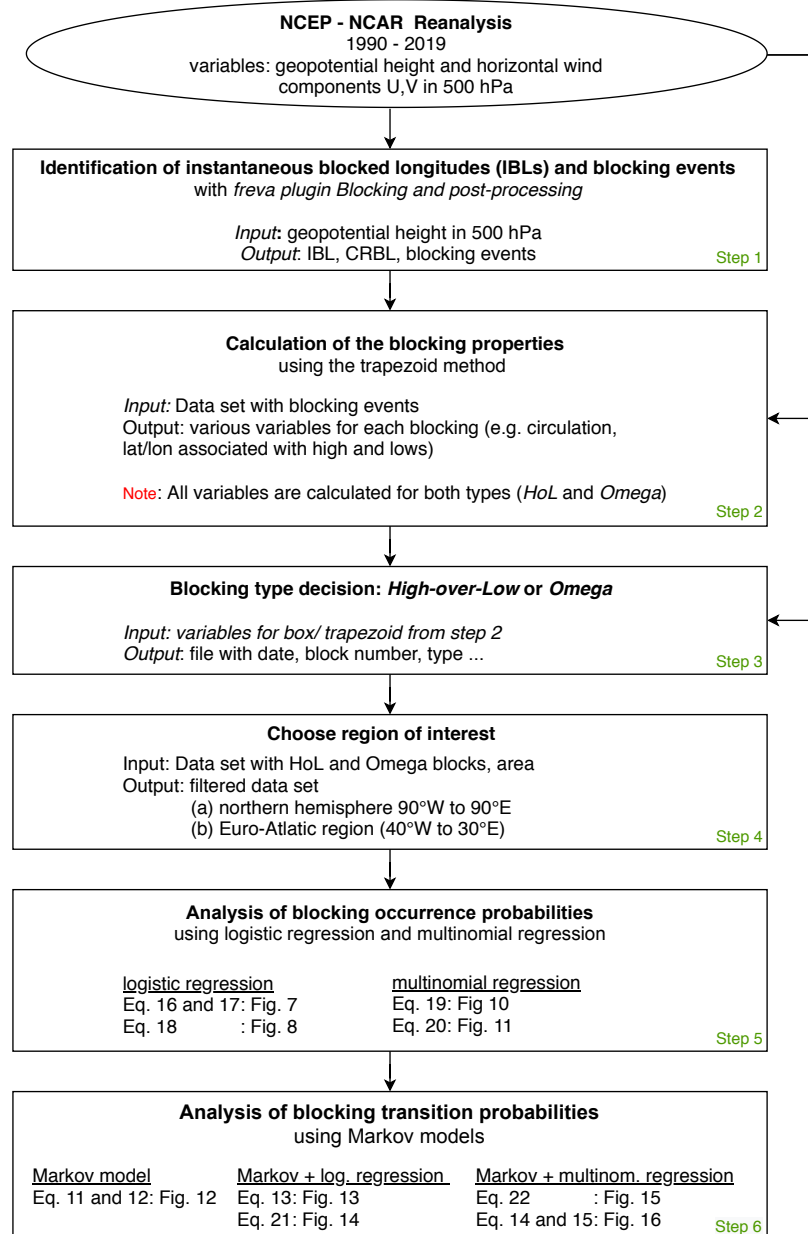
The work is structured as follows. First, we shortly describe the data set and variables that will be used for our analysis in section 2. In section 3, we will explain the steps of our method in more detail: This includes the identification of blocking events (section 3.1) and their properties (section 3.2). Moreover, the decision process for the blocking types – *High-over-Low* or

85 *Omega* block – is explained in section 3.3. We use a subset of the blocking data (section 3.4) in order to analyse the European-Atlantic region with respect to the evolution and transition probabilities of blocking. The statistical methods used in the analysis of occurrence probabilities (logistic regression) and for the transition probabilities (Markov processes) are explained in sections 3.5 and 3.6. The results will be presented in section 4 and discussed in section 5. A final concise conclusion is given in section 6.

2 Data

90

We used the NCEP-DOE Reanalysis 2 data set (Kanamitsu et al., 2002) for our analysis. The data has a grid spacing of $2.5° \times 2.5°$ on a regular latitude/longitude grid and is available every 6 hours. In our study, we used a period of 30 years from 1990 to 2019. We restricted the analysis to the 500 hPa level, a level where the divergence of the wind field is very low (Schielicke, 2017). This allows us to apply the principles of point vortex theory that requires incompressible flow, i.e. a zero

95 divergence. The variables used for this study were the geopotential height and the horizontal wind components (U, V) at 500 hPa. We will compare the blocking behaviour in two regions. The first region covers half the northern hemisphere from $90° W$ to $90° E$, and the second region is a subset of this larger region covering the Euro-Atlantic area from $40° W$ to $30° E$.

3 Methods and design of study

In the following we describe the data preparation and the methodology for the probabilistic analysis of atmospheric blocking.

100 The steps are summarized in Fig. 2.

Figure 2. Structure diagram of the individual steps of the evaluation as explained in section 3.

3.1 Step 1. Identification of instantaneous blocked longitudes (IBLs) and blocking events

In the first step, we use the *Blocking* plugin (Richling et al., 2015) of the freva system (Freie Universität Berlin Evaluation System, see Freva, 2017) to calculate the so-called instantaneous blocking index. This index is a binary 1d blocking index that determines instantaneous blocked longitudes, short IBLs, for every time step of a data series (here, NCEP-DOE Reanalysis 2). The instantaneous blocking index was developed by Tibaldi and Molteni (1990) and identifies blockings in terms of gradients of the geopotential height with regard to a central reference blocking latitude (CRBL). While the CRBL is fixed to $50° N$ in the original work, the freva Blocking plugin uses a modification (after Barriopedro et al., 2010) that allows for a latitudinal-dependent, temporally-varying CRBL in accordance to the climatological stormtrack. A blocking is identified if the geopotential height gradients on the northern (GHGN) and on the southern (GHGS) side of the CRBL satisfy the following criteria:

$$GHGS > \quad 0 \, \frac{gpm}{°N} \quad : \text{corresponding to an easterly directed flow}$$
$$GHGN < -10 \, \frac{gpm}{°N} \quad : \text{similar to a west wind of 8 m/s} \tag{1}$$

In the calculation performed for this study, the spatiotemporally varying CRBL is determined based on the 30-year climatology (1990-2019) of the 500 hPa geopotential height field. In order to catch blocking that are not directly at the CRBL, a possible shift (Delta) to the north and south is set to 10 degrees latitude in the plugin configuration table. For each time step, we get a (1d) series of longitudes (either 1: blocked or 0: unblocked) that is saved for further analysis. For more details on the method and the specific configurations used in the analysis see the Supplementary Material and Richling et al. (2015).

Prior to the blocking classification, the time series of IBLs is post-processed in the following manner: First, we identify *blocking events* as simply-connected points of IBL = 1 in the time-longitude field. From these blocking events we chose events with a minimum duration of 5 days, i.e. 20 time steps, and a spatial extent of at least 15 degrees longitudes. We only consider northern hemisphere blocks in the longitudinal range of $90° W$ to $90° E$ and north of about $45° N$. Note, that we can have two blocking events at the same time in different parts of the area. If this case occurs, the state of the first block is used for the analysis, since only one state can be assigned per time step for the analysis.

3.2 Step 2. Calculation of the blocking properties with the trapezoid method

The blocking event list derived in step 1 will be used to search for blocking patterns in the corresponding NCEP Reanalysis fields. For this purpose we applied the trapezoid method (Müller et al., 2015; Hirt et al., 2018) that is able to detect *High-over-Low* and *Omega* blocking patterns using aspects of flow kinematics to identify the vortices as well as point vortex theory to determine blocking properties and to classify the blocking type. The idea behind the trapezoid method is that, in a regular lat/lon projection, a *High-over-Low* block resembles a box shape and an *Omega* block resembles a trapezoidal shape where the two lows form the broader base of the trapezoid and the high its smaller top. By assigning specific parts of the trapezoid or box to each low and high, we are able to determine the properties (circulation, location of vortex center) of the associated vortices (cf. Fig. 3 of Müller et al., 2015). We will give a brief overview here.

The highs and lows are detected by an analysis of the kinematics of the flow. Therefor, we use the dimensionless kinematic vorticity number $W_k = \|\mathbf{\Omega}\|/\|\mathbf{S}\|$ (Truesdell, 1953, 1954), which compares the local rates of rotation $\|\mathbf{\Omega}\|$ and strain $\|\mathbf{S}\|$ at each grid point. Here, $\mathbf{\Omega} = [\nabla\mathbf{v} - (\nabla\mathbf{v})^{\mathbf{T}}]/\mathbf{2}$ and $\mathbf{S} = [\nabla\mathbf{v} + (\nabla\mathbf{v})^{\mathbf{T}}]/\mathbf{2}$ denote the antisymmetric and symmetric components of the velocity gradient tensor $\nabla\mathbf{v}$ that describes the kinematic flow properties around a point.
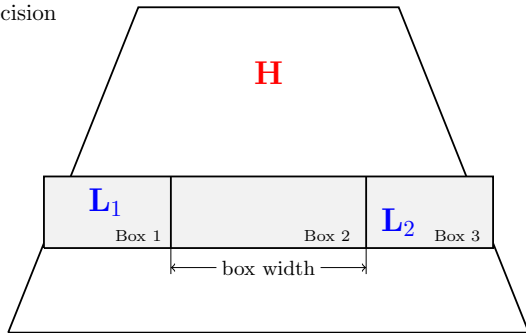
For the calculation of $\|\mathbf{\Omega}\|$, $\|\mathbf{S}\|$ and W_k, we use the two-dimensional, horizontal wind components U, V of the NCEP reanalysis data set at the 500 hPa level. A vortex is then defined as grid point(s) of $W_k > 1$, i.e. as an area where the rotation-rate prevails over the strain-rate (see Schielicke et al., 2016; Schielicke, 2017, for further insight and more atmospheric applications). On the other hand, all grid points of $W_k \leq 1$ are set to zero. Hence, the kinematic vorticity number is used to generate a field of vortex patches. In this field, we search for the high that lies closest to the longest-blocked IBL. Initially, this high is enclosed by a box shape such that its circulation magnitude is maximized. Subsequently, the box/trapezoid is step-by-step increased equatorwards (additionally west-/eastward in case of the trapezoid) until the total circulation inside the shape is close to zero (for more details, see Hirt et al., 2018). This is in accordance with point vortex theory, which states that a system of two or three vortices moves westward if the sum of their circulations is zero, the high lies polewards of the low(s), and the 3-point-vortex-system forms an equilateral triangle (Müller et al., 2015). Note, that we determine the box associated with the *High-over-Low* pattern as well as the trapezoid with the *Omega* pattern for each time step separately. Moreover, for each pattern a number of block properties such as the circulations, and the latitude and longitude associated with the high and the lows are derived for later analysis. The decision, which blocking type pattern better fits, is done directly after the calculation of the trapezoid and box shape and is described in the following step 3.

3.3 Step 3. Blocking type decision: *High-over-Low* or *Omega* blocking
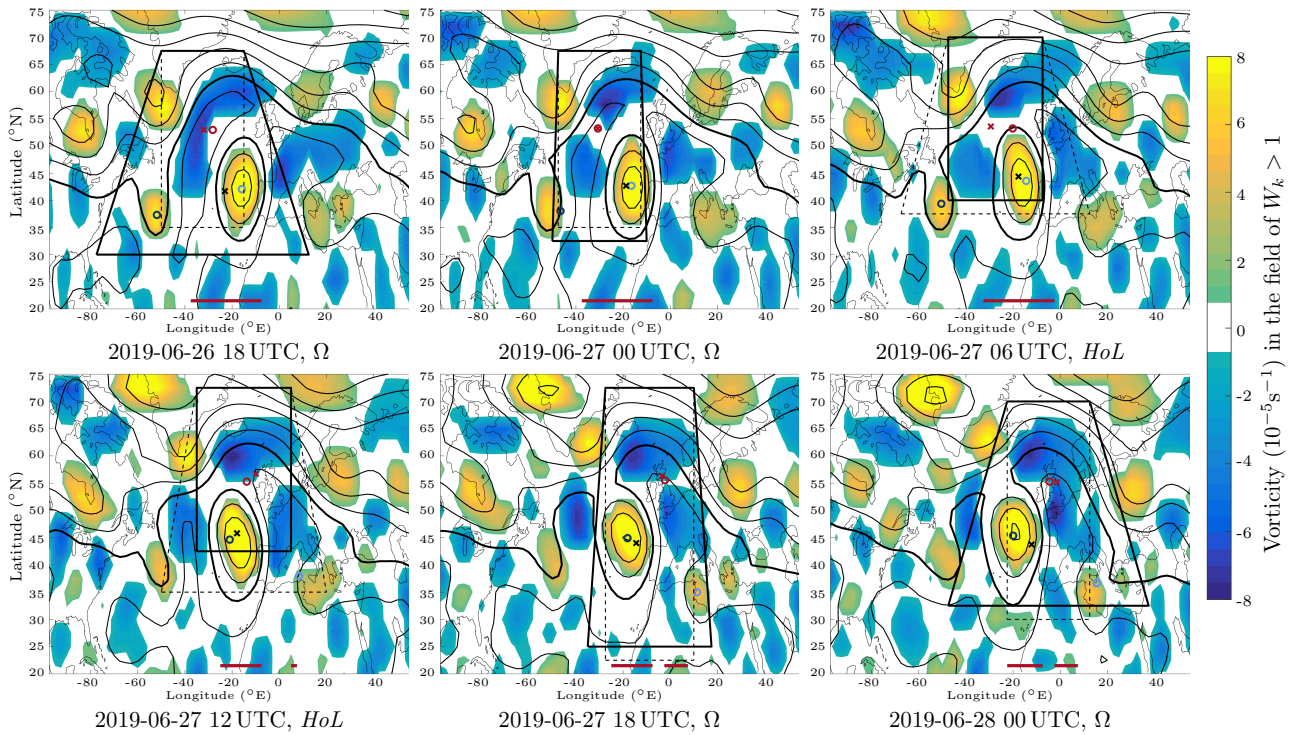
For the blocking type decision, we inspect the trapezoid and the box shape derived in step 2 for each time step. Therefor, the area below the high center around the mean latitude of the lows (trapezoidal shape) is inspected as follows: A rectangle is centered around the longitude of the high and mean latitude of the lows and split in 3 smaller rectangles where the middle one has a width of 25 degrees longitude and the two outer rectangles are limited by the outline of the trapezoid (see Fig. 3a). If the mean vorticity inside the middle rectangle (Box 2 in Fig. 3a) is higher (lower) than the mean vorticity of all three rectangles together, the timestep is defined as *High-over-Low* (*Omega*) block. Finally, we have a time series of each blocking event that can contain both blocking types within a single blocking event (for an example see Fig. 3b and Supplementary Material). This is a new addition to the trapezoid method in Hirt et al. (2018), where we assigned a single blocking type to each whole blocking period. Finally, the time series is once more checked for consistency: In our analysis, a blocking event is expected to consist of the same anticyclone. Hence, large jumps in the locations of a high from one time step to the next one are regarded as a new blocking event and the old event will be split into two events. If the lifetime of one or both events becomes less than 5 days, the event(s) is(are) removed from the analysis.

(a) Sketch of blocking type decision

(b) Example blocking event for selected time steps

Figure 3. (a) Schematic representation of the blocking type decision based on the trapezoid method. The positive vorticity is calculated for all three boxes, which lie on the mean latitude of the low pressure areas (L_1, L_2). Depending on the magnitude of the mean vorticty in these three boxes, the decision between *High-over-Low* and *Omega* is made. (b) An example blocking event, observed at 26. June 2019 18 UTC - 28. June 0 UTC, is plotted for six time steps that include a transition between *Omega* and *High-over-Low* blocking states. Shaded areas represent the identified vortex field ($W_k > 1$) which is colored by vorticity (in $10^{-5} s^{-1}$; blue: anticyclonic; yellow cyclonic). Black contours are isolines of geopotential height in 80 gpm intervals (thick black contour is the 5840 gpm isoline). The outline of the trapezoid/box is given for each time step, solid shape represent the identified shape; circles (crosses) are the circulation centroids of the identified high (red) and low(s) (blue) for the *Omega* (*High-over-Low*) pattern. The red bar(s) at the bottom of the figures shows the identified IBLs from Step 1. The figures were plotted with help of Matlab (2016) and coastlines were plotted with the built-in Matlab file *coast.mat*. The full time series is given in the Supplementary Material, see also steps 2 and 3.

3.4   Step 4. Choose region of interest: Europe-Atlantic region and half northern hemisphere

The blocking data set derived after applying step 1 to 3 is composed of blocking events that occur between $90°\,W$ and $90°\,E$

165   with a life time of at least 5 days (= 20 time steps). The detected high centers lie in the mid-latitudes between about $44.5°\,N$

and $83°\,N$. To analyse blocking in Europe in more detail, we separated this data set in a second subset: the Euro-Atlantic sector

ranging from $40°\,W$ to $30°\,E$. Since this is a subset of the larger blocking event list, blocks with life times smaller than 5 days

can occur in this region. At some point in their life time, these blocks move in or out of the European sector.

3.5   Step 5. Analysis of blocking occurrence probability using logistic regression

170   Logistic regression is designed to model probabilities ($0 \leq p \leq 1$) and is an adequate model to describe blocking occurrence

probabilities and their temporal changes for a system that can only yield two states: in our case *blocking* and *no-blocking*

patterns. The occurrence probabilities for a system with three possible states: *unblocked* and two distinct blocking states

(*Omega* and *High-over-Low*), can be analogously described with multinomial regression. Both are briefly reviewed here.

Logistic regression is a special case of generalized linear models (e.g., Wilks, 2011; Dobson and Barnett, 2008) designed to

175   describe occurrence probabilities depending on a set of external influences (covariates). These covariates can be, for example,

time in years as a proxy for climate change, the season or month of occurrence as a proxy for the seasonal cycle, or also

large-scale atmospheric flow variables.

The setting can be viewed as a generalization to standard linear models. Let Y_t be a discrete random variable at discrete times

t; observations of Y_t are denoted as y_t. The random variable Y_t describes the discrete states of a Markov chain. The two-state

180   model we begin our analyses with, is based on these two states: *no blocking* (nB) and *blocking* (B), observations (coded in

integers) can thus only be $y_t = 0$ for nB and $y_t = 1$ for B. The random variable Y_t follows a binomial distribution completely

determined by the expectation value which gives the occurrence probability of the blocking event $E[Y_t] = Pr\{Y_t = 1\} = p_t$.

The probability of the state *no blocking* is determined by the counter-probability $Pr\{Y_t = 0\} = 1 - p_t$.

Logistic regression describes the dependence of the blocking occurrence probability p_t at time t as a function of covariates

185   $x_{l,t}$ using a log-odds (or logit) link-function

$$\mathrm{logit}(p_t) = \ln\left(\frac{p_t}{1 - p_t}\right) = \beta_0 + \Sigma_{l=1}^{L}\beta_l\, x_{l,t}\,, \tag{2}$$

with $l = 1, \ldots, L$ covariates $x_{l,t}$ observed simultaneously with y_t; β_l are model parameters to be estimated based on iteratively

reweighted least-squares (IRLS). Further details can be found, e.g., in Dobson and Barnett (2008); Wilks (2011). We use the

function `glm()` from the package `stats` of the R-environment for statistical computing (R Core Team, 2018).

190   Rearranging Eq. (2) yields the following expression for the blocking occurrence probability at time t as a function of the

covariates $x_{l,t}$:

$$p_t = \frac{1}{1 + e^{-(\beta_0 + \Sigma_{l=1}^{L}\beta_l x_{l,t})}}\,. \tag{3}$$

In some cases, the influence of one covariate $x_{i,t}$ dependents on the value of another covariate $x_{j,t}$ which can be introduced

in a linear model as a so called *interaction* effect $x_{i,t}\, x_{j,t}$. Think of, for example, the change in blocking occurrence probability

195   with years is dependent on the season, we are looking at. A simple example with *main effects* of two covariates and one
interaction is

$$\text{logit}(p_t) = \beta_0 + \beta_1 x_{1,t} + \beta_2 x_{2,t} + \beta_3 x_{1,t} x_{2,t}. \tag{4}$$

In the notation for generalized linear models introduced by McCullagh and Nelder (1989) Eq. 4 reads

$$\text{logit}(p_t) \sim x_{1,t} * x_{2,t} \sim x_{1,t} + x_{2,t} + x_{1,t} : x_{2,t}, \tag{5}$$

200   with $x_{i,t}$ denoting main effects, $x_{1,t} : x_{2,t}$ interaction effects and $x_{1,t} * x_{2,t}$ their commonly used combination. This notation
assumes an offset (β_0) being present by default and a parameter β_i to be estimated for each term in the equation. Nota bene: in
this notation, the symbols '+', ':' and '*' have special meanings, namely addition of a term in the predictor, interacting effects
and combination of both, respectively!

For more than two states, the model can be extended to multinomial logistic regression. We next consider a multinomial
205   random variable Y_t with three states: no blocking (nB), *High-over-Low* (HoL) and *Omega* blocking (Ω). For the multinomial
distribution, one probability, e.g. $Pr\{Y_t = nB\} = p_{nB,t}$, is set as reference and the other two $Pr\{Y_t = HoL\} = p_{HoL,t}$ and
$Pr\{Y_t = \Omega\} = p_{\Omega,t}$ need to be estimated using

$$\ln\left(\frac{p_{HoL,t}}{p_{nB,t}}\right) \sim x_{1,t} + x_{2,t} + \ldots \tag{6}$$

$$\ln\left(\frac{p_{\Omega,t}}{p_{nB,t}}\right) \sim x_{1,t} + x_{2,t} + \ldots. \tag{7}$$

210   The remaining occurrence probability for no blocking can then be derived as $p_{nB,t} = 1 - (p_{\Omega,t} + p_{HoL,t})$. We thus need to
solve two regression equations simultaneously. Parameter estimation is somewhat more cumbersome in this case and detailed
in (Yee, 2015). Estimation is carried out using the function `multinom()` from the R-package VGAM (Yee, 2015).

3.6   Step 6. Analysis of blocking transition probabilities using Markov models

We use Markov models with two and three states to describe transition probabilities between the states related to the different
215   blocking types and the no-blocking state. For both cases, there is thus a discrete set of possible states:

two-state model: *blocked* (B) and *unblocked* (nB) states,

three-state model: *High-over-Low* (HoL), *Omega* (Ω) and *unblocked* (nB) states.

The system evolves along a discrete time axis t and can switch between these discrete states. We obtain a *discrete-time*
Markov chain on a finite state space. The underlying theory was developed by the Russian mathematician Andrey Andreyevich
220   Markov.

Let Y_t be a sequence of discrete random variables denoting the possible states the Markov chain can be found in, e.g.,
$Y_t = i$ implies Y being in state i at time t, in general $i \in \{1, 2, 3, \ldots, I\}$, here, $I = 2$ or $I = 3$ for the two-state-model or three-
state-model, respectively. We speak of a transition when $Y_{t-1} = i$ changes to $Y_t = j$. Transitions from $Y_{t-1} = i \rightarrow Y_t = j$ are

described with conditional probabilities which, in general, depend on the history of the process, i.e.

225
$$p_{ij,t} = P(Y_t = j \mid Y_{t-1} = i, Y_{t-2}, Y_{t-3}, \ldots). \tag{8}$$

Formally, $Y_{t-1} = i \rightarrow Y_t = i$ is also called a transition from state i to itself. The Markovian assumption (or Markov property) requires these transition probabilities to depend only on the actual state and not the full history of the process

$$p_{ij,t} = P(Y_t = j \mid Y_{t-1} = i, Y_{t-2}, Y_{t-3}, \ldots) = P(Y_t = j \mid Y_{t-1} = i). \tag{9}$$

This assumption makes handling these processes a lot easier. For *homogeneous* Markov chains, the transition probabilities
230 are independent of external factors or time, i.e. $p_{ij,t} = p_{ij}$, otherwise we speak of a *non-homogeneous* Markov chain. The probability for finding the system at time t in state j, i.e. $Pr\{Y_t = j\}$, is determined by the transition probabilities p_{ij} from all states i into state j weighted with the probability $Pr\{Y_{t-1} = i)$ of finding the system in state i, thus

$$Pr\{Y_t = j\} = \sum_i Pr\{Y_t = j \mid Y_{t-1} = i\} Pr\{Y_{t-1} = i) = \sum_i p_{ij,t} Pr\{Y_{t-1} = i\}. \tag{10}$$

The simplest Markov Chain is a Bernoulli process consisting of two states, in our case the two-state-model with no blocking
235 (nB) and blocking (B) ($i,j \in \{nB, B\}$) with transition probabilities given in the transition matrix

$$M_2 = \begin{pmatrix} p_{nB,nB} & p_{nB,B} \\ p_{B,nB} & p_{B,B} \end{pmatrix} \tag{11}$$
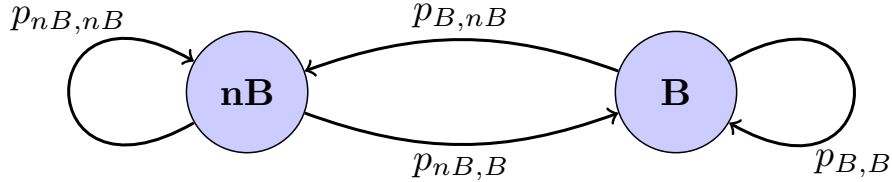
with $p_{nB,B} = Pr\{Y_t = B \mid Y_{t-1} = nB\}$. For the three-state-model (*High-over-Low blocking* (HoL), *Omega* blocking (Ω) and *no-blocking* (nB), $i,j \in \{nB, HoL, \Omega\}$), the transition matrix is

$$M_3 = \begin{pmatrix} p_{nB,nB} & p_{nB,HoL} & p_{nB,\Omega} \\ p_{HoL,nB} & p_{Hol,HoL} & p_{HoL,\Omega} \\ p_{\Omega,nB} & p_{\Omega,HoL} & p_{\Omega,\Omega} \end{pmatrix}. \tag{12}$$

240 Transition probabilities are between 0 and 1 ($0 \leq p_{ij} \leq 1$) and rows sum up to unity, implying that the probability that any of the possible states i is reached at time $t + 1$ is one. Transition probabilities together with the probability distribution of Y_0 (initial distribution) fully describe the Markov chain.

Homogeneous (time-independent) Markov chains can be illustrated using a network diagram. Figure 4 shows an example with two states. The circles describe the different states and the arrows indicate the direction of the transition with the
245 corresponding transition probability p_{ij}. In the homogeneous case, transition probabilities can be estimated from relative frequencies. A more general description of Markov chains and their matrices of transition probabilities can be found in Chap. 9.2 in Wilks (2011). More examples of atmospheric applications of (finite-state) Markov chains can be found in Gottwald et al. (2016, Chapt. 3.4). For further details on homogeneous Markov processes, see (e.g., Baclawski, 2008).

For a non-homogeneous (time-dependent) Markov-process, we use logistic regression to estimate time varying transition
250 probabilities. For the two-state model with blocking ($Y_t = B$) and no blocking ($Y_t = nB$), we describe transition probabilities

Figure 4. A general example of a network diagram of a homogeneous Markov chain with two states nB (*no blocking*) and B (*blocking*). Arrows indicate transitions and p_{ij} the associated transition probabilities between state i and j with $i, j \in \{nB, B\}$. After Baclawski (2008).

changing with Year as

$$\text{logit}(P(Y_t = B \mid Y_{t-1})) \sim Y_{t-1} * \text{Year}, \tag{13}$$

using the notation for generalized linear models introduced above. This results in probabilities for blocking conditioned on being in an unblocked state $Pr\{Y_t = B \mid Y_{t-1} = nB\}$ and conditioned on being in a blocked state $Pr\{Y_t = B \mid Y_{t-1} = B\}$ varying in time. So do their counter probabilities $Pr\{Y_t = nB \mid Y_{t-1} = nB\} = 1 - Pr\{Y_t = B \mid Y_{t-1} = nB\}$ and $Pr\{Y_t = nB \mid Y_{t-1} = B\} = 1 - Pr\{Y_t = B \mid Y_{t-1} = B\}$. Analogously, we can describe time-varying (with Year and Seas) transition probabilities for the three-state model using multinomial logistic regression, setting the reference to $Pr\{Y_t = nB \mid Y_{t-1}\}$ and
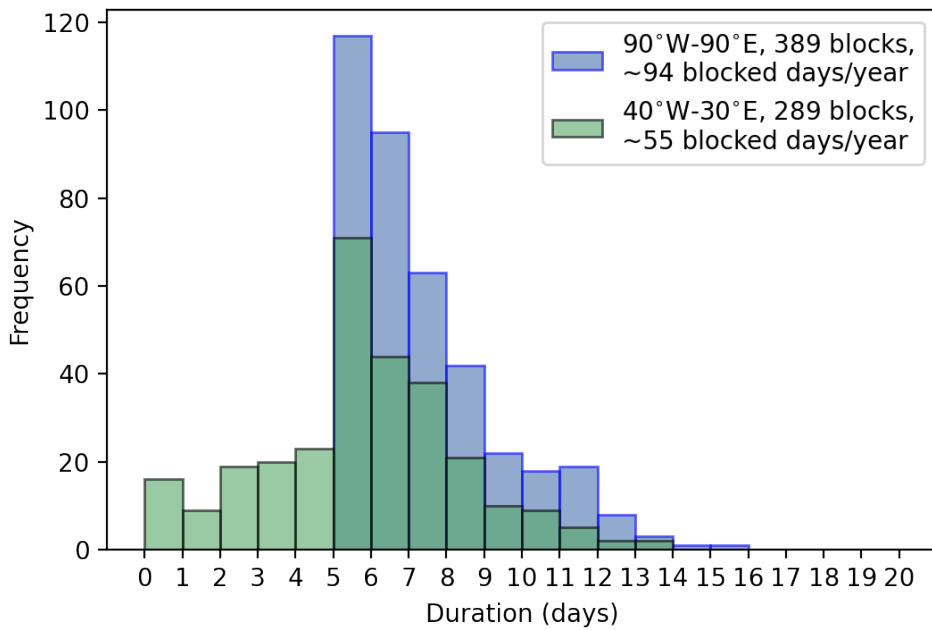
$$\ln \left(\frac{Pr\{Y_t = HoL\} \mid Pr\{Y_{t-1}\}}{Pr\{Y_t = nB \mid Y_{t-1}\}} \right) \sim Y_{t-1} * \text{Year} * \text{Seas}, \tag{14}$$

$$\ln \left(\frac{Pr\{Y_t = \Omega\} \mid Pr\{Y_{t-1}\}}{Pr\{Y_t = nB \mid Y_{t-1}\}} \right) \sim Y_{t-1} * \text{Year} * \text{Seas}. \tag{15}$$

Probabilities for all transitions can be derived with the condition $Pr\{Y_t = HoL\} + Pr\{Y_t = \Omega\} + P\{Y_t = nB\} = 1$. For details on main and interaction effects with categorical terms in the predictor, see Wilks (e.g., 2011); Dobson and Barnett (e.g., 2008).

4 Results

The results are divided into three sections. First the relative frequencies of the two-states model (*blocking, no blocking*) are considered. Here, the temporal development as well as the seasonal and monthly changes are considered. In the second section this analysis is shown for the division into three states (*no blocking, Omega, High-over-Low*). In the last part the transition probabilities of two and three states are discussed. These are also analyzed and shown in their temporal evolution.
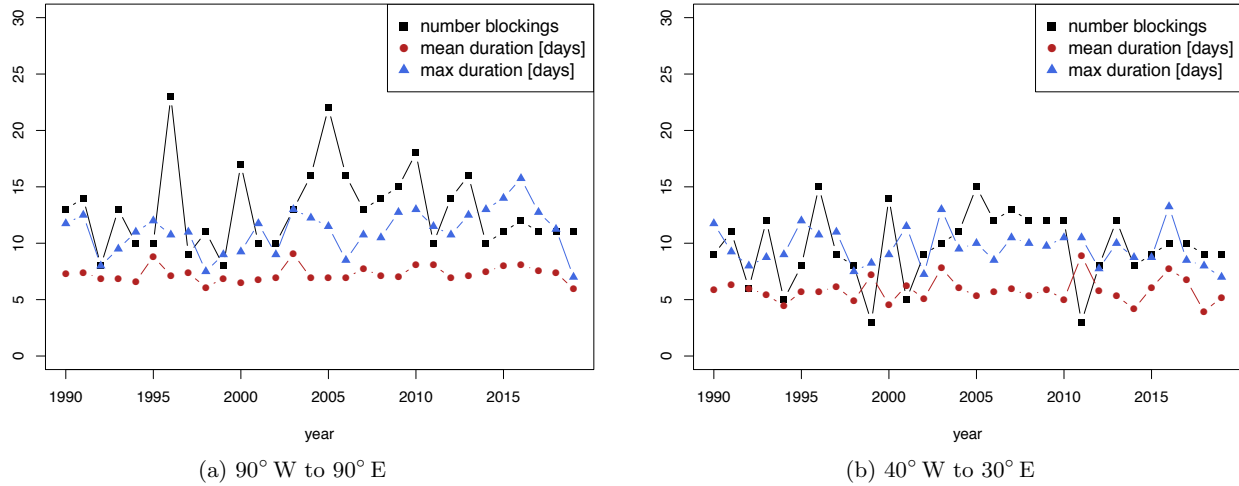
Figure 5. Histogram of the duration of all blocking events for two selected regions: blue: northern hemisphere ($90° W$ to $90° E$), green: Euro-Atlantic region ($40° W$ to $30° E$).

4.1 Temporal development of blocking probabilities – Two-states blocking model

4.1.1 Duration of blocking events

Figure 5 shows the frequency distribution of durations of blocking events. In the 30-year period from 1990 to 2019 in the

270 region $90° W$ to $90° E$ (northern hemisphere), we detect a total of 389 blocks ($\approx$13 blocks per year) that lasted for five or more days (see Fig. 5, blue columns) with an average of about 94 blocked days per year. Out of the 389 blocks, the Euro-Atlantic region ($40° W$ to $30° E$) was affected by 289 blocks for at least some of the lifetime of the blocks with an average of about 55 blocked days per year. Since the Euro-Atlantic blocks are a subset of the blocks that occur in the larger region, blocking lifetimes can be smaller than 5 days. However, only 87 of the 289 blocks remained less than 5 days in the Euro-Atlantic region,

275 while the majority affected the region for 5 to 8 days (153 blocks, see Fig. 5, green columns). Since blocks are observed to be quasi-stationary with usually low travel speeds, the small number of short-lived blocks in the Euro-Atlantic region probably start or end close to the region boundaries and move either in or out of the region during their life time.

(a) $90° W$ to $90° E$ (b) $40° W$ to $30° E$
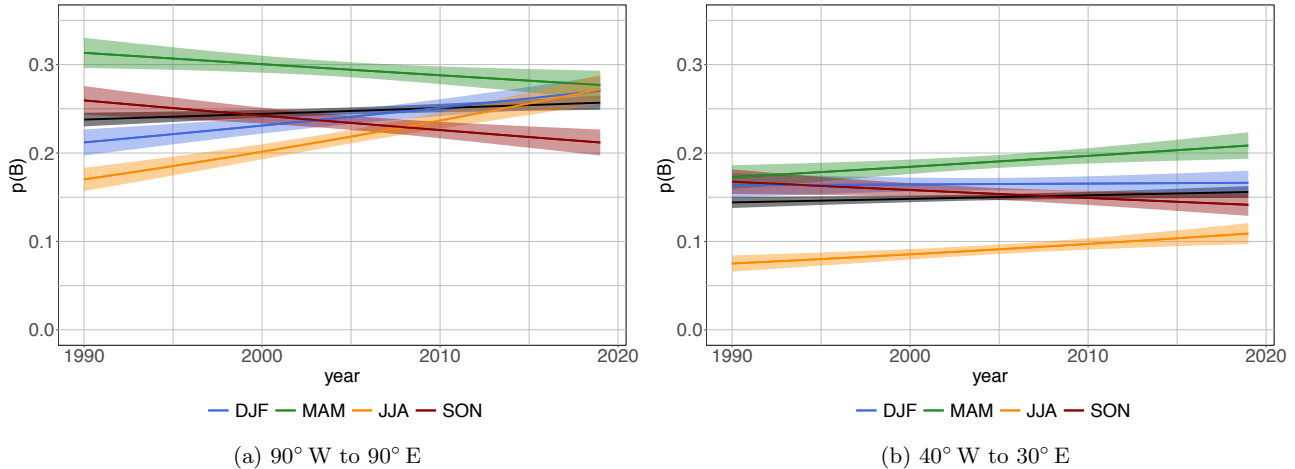
Figure 6. Temporal development of frequency, average and maximum duration of a blocking event (a) for the whole domain ($90° W$ to $90° E$) and (b) for Euro-Atlantic region ($40° W$ to $30° E$).

4.1.2 Temporal development of blocking frequency and duration

The temporal development of the blocking frequency and duration is shown in Fig. 6: On the left hand side the whole domain

280 from $90° W$ to $90° E$ is shown; and on the right hand side we concentrate on the temporal developments in the Euro-Atlantic sector ($40° W$ to $30° E$). In both regions, we observe over the 30 years no clear trend in the frequency of detected blocking events, however, the observed year-to-year variability is high (see black squares in Fig. 6). A straight-line fit shows just a slight total increase of 0.15 blocks over the 30 years (not shown) with a mean number of 13.2 blocks per year ($90° W$ to $90° E$), and and increase of 0.55 blocks in 30 years with a mean number of 9.8 blocks per year ($40° W$ to $30° E$), respectively. The mean

285 duration of the blocking events increases slightly in both regions with an increase of 0.3 days (0.4 days) over the 30 year periods in $90° W$ to $90° E$ with a mean duration of 7.3 days ($40° W$ to $30° E$ with mean duration of 7.2 days) which corresponds to a total increase of about one to two time steps in 30 years (see red circles in Fig. 6). However, the estimated slopes are close to zero (not shown). The strongest positive tendency is observed for the development of the maximum duration of the blocking events in $90° W$ to $90° E$ with an increase of 2.1 days, i.e. 8 to 9 time steps, over 30 years (averaged maximum duration is 11.1

290 days). This can be attributed to blocks that occur over (western) Russia. While there is nearly no increase (≈ 0.05 days in 30 years) in the maximum duration observed in the Euro-Atlantic region (averaged maximum duration is here 10.3 days).

4.1.3 Seasonal blocking probability

Figure 7 shows the temporal evolution of blocking probability, i.e. the probability of a time step being part of blocking event that lasted a minimum of 5 days, for the 30 year period separated by year and season. Probability is obtained with the logistic

(a) $90° \, W$ to $90° \, E$ (b) $40° \, W$ to $30° \, E$

Figure 7. Blocking probability over time for the full *year* (black line, Eq.16) and for individual *seasons* (colored lines, Eq. 17). Shadings shows 95% confidence intervals. (a) $90° \, W$ to $90° \, E$ and (b) selected Euro-Atlantic region ($40° \, W$ to $30° \, E$).
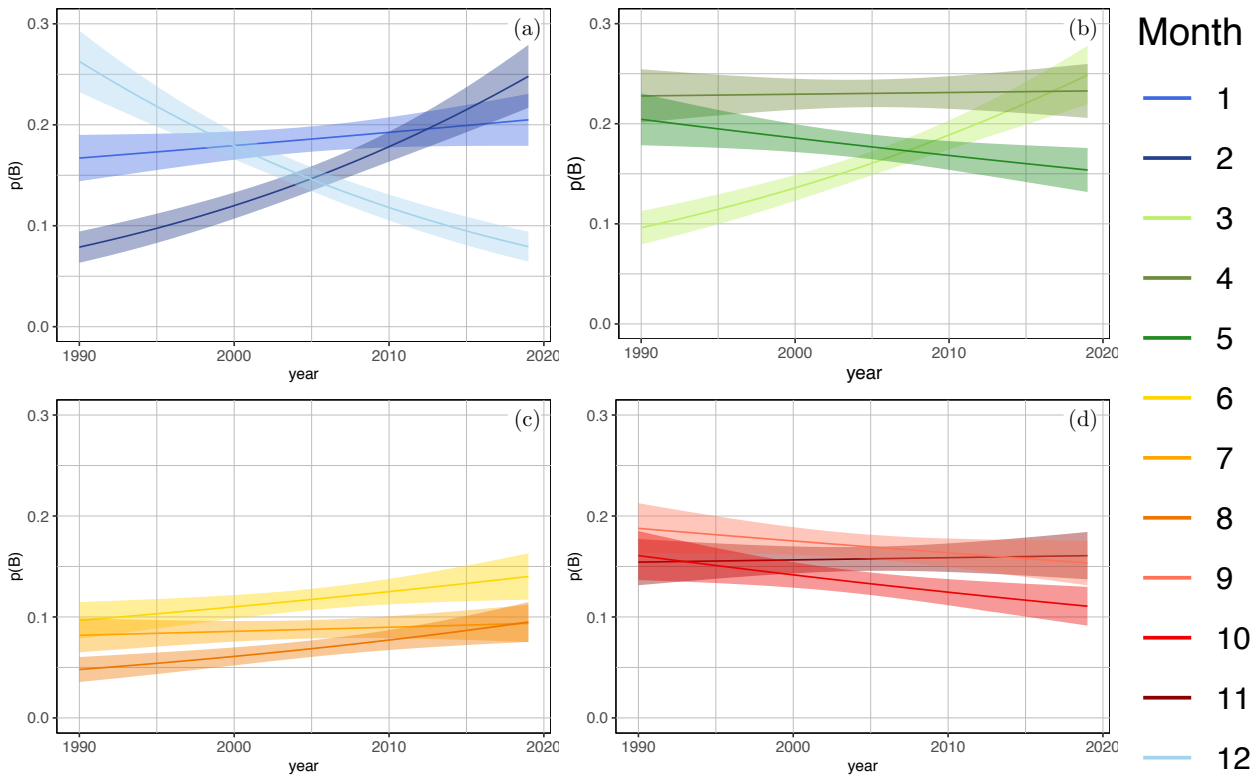
295   regression models using $\text{Seas} \in \{\text{DJF}, \text{MAM}, \text{JJA}, \text{SON}\}$ as a categorical term in the predictor

$$\text{logit}(p) \sim \text{Year}\,, \tag{16}$$

$$\text{logit}(p) \sim \text{Year} * \text{Seas}\,. \tag{17}$$

where the months December, January, February, etc. have been abbreviated by capital letters D, J, F, and so forth. The black lines in Fig. 7 show the probabilities for the full year (Eq. 16) and are thus comparable to the straight-line estimates in

300   Sec. 4.1.2. The colored lines show the development of the blocking probability in the individual seasons using an interaction effect (Eq. 17). Within the study period, the annual blocking probability increases from about $p = 0.24$ ($p = 0.145$) in 1990 to almost $p = 0.26$ ($p = 0.155$) in 2019 for the whole domain (Euro-Atlantic region). Average probability is about 25% blocked time steps in $90° \, W$ to $90° \, E$ and about 15% blocked time steps in $40° \, W$ to $30° \, E$.

     Using season as interaction effect in the regression (Eq. 17) reveals that this increase over the 30 years stems to a large

305   extend from a strong increase in the summer months (JJA) from $p \approx 0.17$ to $p \approx 0.27$ of blocked time steps for $90° \, W$ to $90° \, E$, and $p \approx 0.075$ to $p \approx 0.11$ for $40° \, W$ to $30° \, E$, respectively. Furthermore, in the region $90° \, W$ to $90° \, E$, the probability of blocked time steps in winter (DJF) increase, too, from $p \approx 0.21$ to $p \approx 0.27$, while the probability of blocked days in the transitional seasons decrease from $p \approx 0.31$ in 1990 to $p \approx 0.28$ in 2019 for spring (MAM) and from $p \approx 0.26$ to $p \approx 0.21$ for autumn (SON) in the same period (Fig. 7, left). Although the spring (MAM) blocked-time steps probability decreases in the

310   full study-region, we observe a significant increase in the Euro-Atlantic region from about 17.5% in 1990 to about 21% in 2019 (Fig. 7, right). In agreement with the larger area, the probability of a blocked day in autumn (SON) decrease from $p \approx 0.0165$ in 1990 to $p \approx 0.014$ in 2019 in the Euro-Atlantic region.

Figure 8. Blocking probability over time for individual month (Eq. 18). Shadings show 95 % confidence intervals. (a) winter (DJF) (b) spring (MAM) (c) summer (JJA) and (d) autumn (SON) in the Euro-Atlantic region ($40° W - 30° E$).
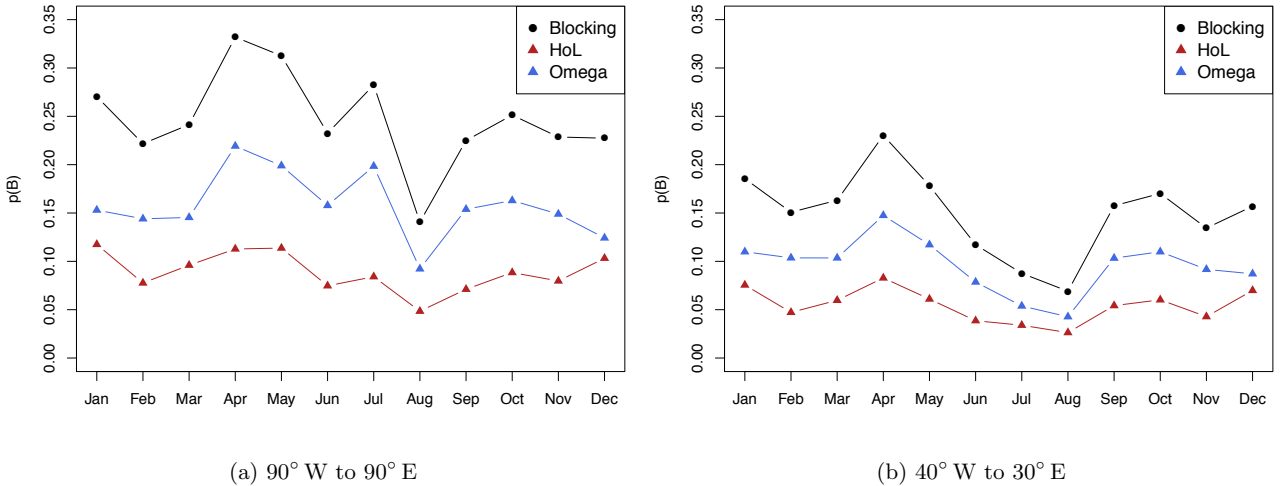
4.1.4 Monthly blocking probability in the Euro-Atlantic region

With a categorical term $\mathrm{Mon} \in \{1, 2, 3, \ldots, 12\}$ in the predictor, interacting with Year

$$\mathrm{logit}(p) \sim \mathrm{Year} * \mathrm{Mon}, \tag{18}$$

we have more temporal detail and can pinpoint the drivers of the observed trends in blocking probability in the Euro-Atlantic sector down to specific months (see Fig. 8).

All summer months, especially June and August, show a slight, but steady increase of blocking probability (see Fig. 8c) and contribute likewise to the observed general increase in summer (Fig. 7 right, yellow-orange line). Similarly, the general decrease of blocking observed in autumn (SON) is mirrored in all months, too, especially in September and October (Fig. 8d). On the other hand, the winter half year shows more disagreements. E.g., we observe an increase in Spring (MAM) on a seasonal basis. This increase can mainly be attributed to a strong increase of blocked time steps in March from about 10% blocked time

(a) $90° W$ to $90° E$ (b) $40° W$ to $30° E$

Figure 9. Blocking probability estimated for individual months for blocking in general, as well as separately for *High-over-Low* and *Omega*. (a) whole domain ($90° W$ to $90° E$) and (b) Euro-Atlantic subsection ($40° W$ to $30° E$).

steps in 1990 to about 25% in 2019. While April is relatively stable over the whole period, we observe a decrease of blocked time steps for May. However, this decrease is smaller in magnitude (from about 20% to about 15%) than the increase in March.
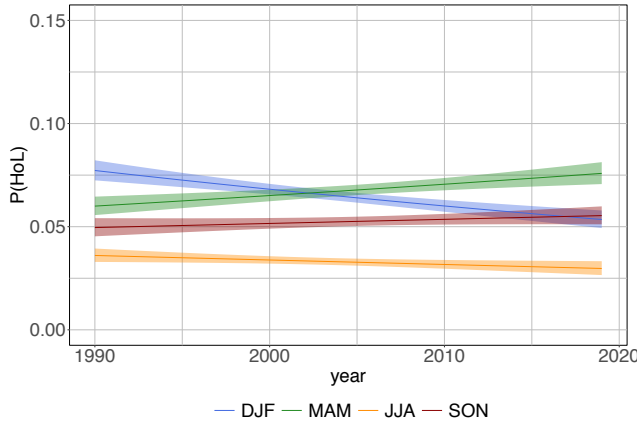
325   The winter months (DJF) show no clear trend over the 30-year period on a seasonal basis (Fig. 7 right, blue line). But the single months show a different behaviour (Fig. 8a): While blocked time steps in December decrease strongly from about $p \approx 0.26$ in 1990 to about $p \approx 0.08$ in 2019, the probability for blocked time steps in February increases strongly (from $p \approx 0.08$ to $p \approx 0.25$, same period) and that for January increase only slightly from $p \approx 0.17$ to $p \approx 0.205$.

4.2 Temporal development of blocking probabilities – Three-states blocking model
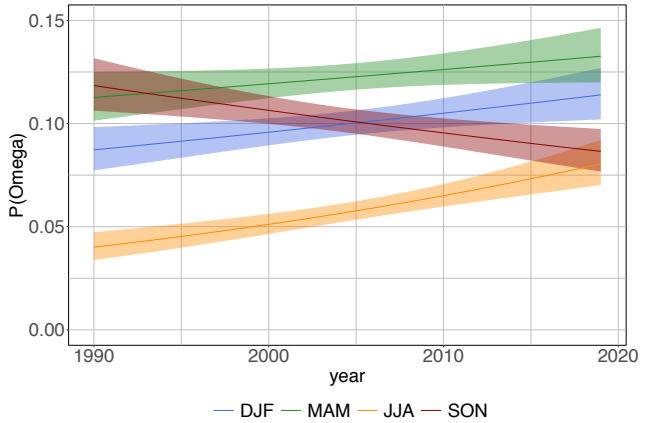
330   In the following, we describe blocking using the three-states blocking model with distinct *High-over-Low* and *Omega* block.

4.2.1 The annual cycle of blocking probability

Figure 9 shows the annual cycle of blocking probability. Taking a look at the individual months reveals that the winter season from September to March is characterized by relatively high blocking probabilities with $\approx 22\%$ ($\approx 15\%$) in $90° W$ to $90° E$ ($40° W$ to $30° E$) and a smaller peak in January (see Fig. 9). The main peak in both regions occurs in April. While the larger

335   region ($90° W$ to $90° E$) has a broader peak with high values in May and a secondary peak in July, the Euro-Atlantic region only peaks in April and shows a broader minimum in June to August. In the larger region, the lowest blocking probability occurs in August, and the peak in July can mainly be attributed to blocking that occurs over (western) Russia (not shown). About

(a) High-over-Low blocking, $40°\,W$ to $30°\,E$ (b) Omega blocking, $40°\,W$ to $30°\,E$

Figure 10. Temporal development for individual seasons (Eq. 19) for the blocking probabilities for the Euro-Atlantic region ($40°\,W - 30°\,E$) for (a) *High-over-Low* and (b) *Omega* blocking.

2/3 of the blocked time steps can be classified as *Omega* blocks and the rest as *High-over-Low* blocks. Only in December and January, this classification rather changes to about 1/2 (both regions, red/blue triangles in Fig. 9).

340   **4.2.2   Seasonal and monthly blocking probability in the Euro-Atlantic sector**
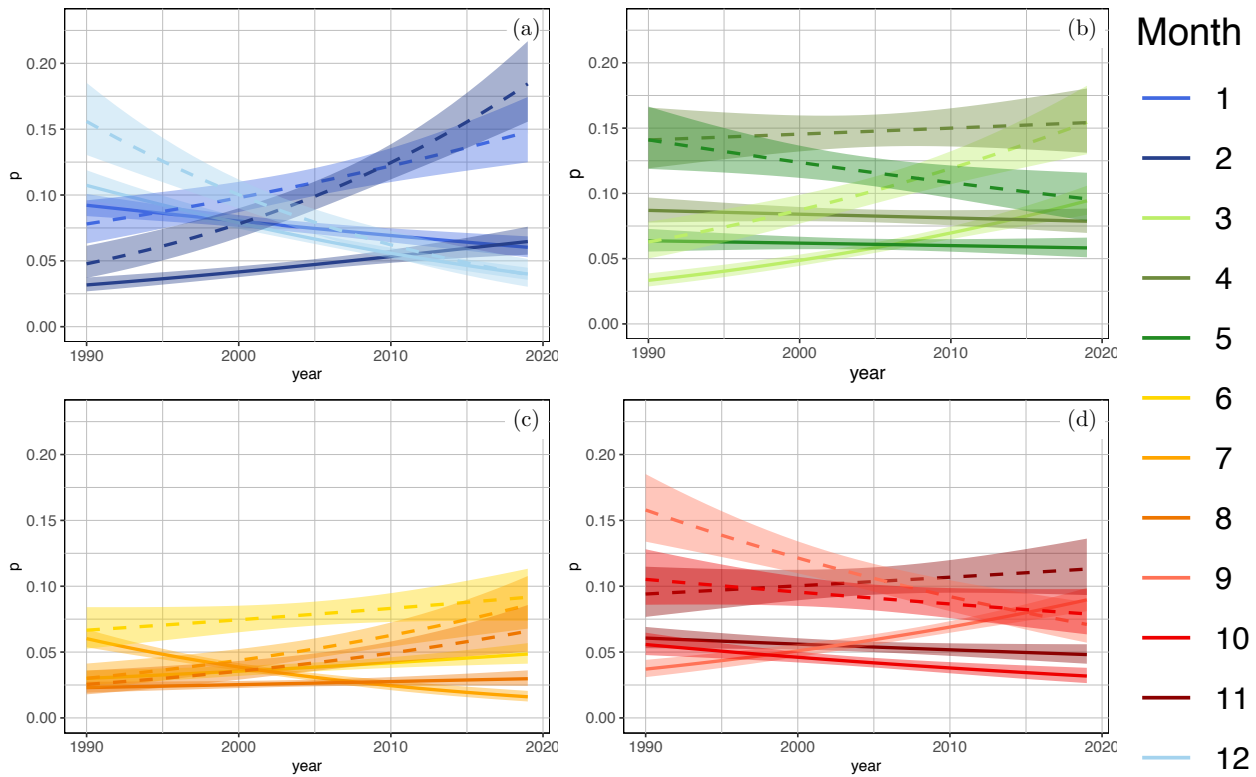
The three-state blocking model with distinct *High-over-Low* and *Omega* block can be described in a similar manner as the two-state model but using multinomial logistic regression (Sec.3.5) with reference $Pr\{Y_t = nB|Y_{t-1}\}$. The models used here are

$$\ln\left(\frac{Pr\{Y_t = HoL\}}{Pr\{Y_t = nB\}}\right) \sim \text{Year} * \text{Seas}, \qquad\qquad \ln\left(\frac{Pr\{Y_t = \Omega\}}{Pr\{Y_t = nB\}}\right) \sim \text{Year} * \text{Seas}, \qquad (19)$$

345   $$\ln\left(\frac{Pr\{Y_t = HoL\}}{Pr\{Y_t = nB\}}\right) \sim \text{Year} * \text{Mon}, \qquad\qquad \ln\left(\frac{Pr\{Y_t = \Omega\}}{Pr\{Y_t = nB\}}\right) \sim \text{Year} * \text{Mon}. \qquad (20)$$

As described in Sec. 3.5, for the both cases, the seasonal and the monthly case, we need two equations, one for $Pr\{Y_t = HoL\}$ and one for $Pr\{Y_t = \Omega\}$.
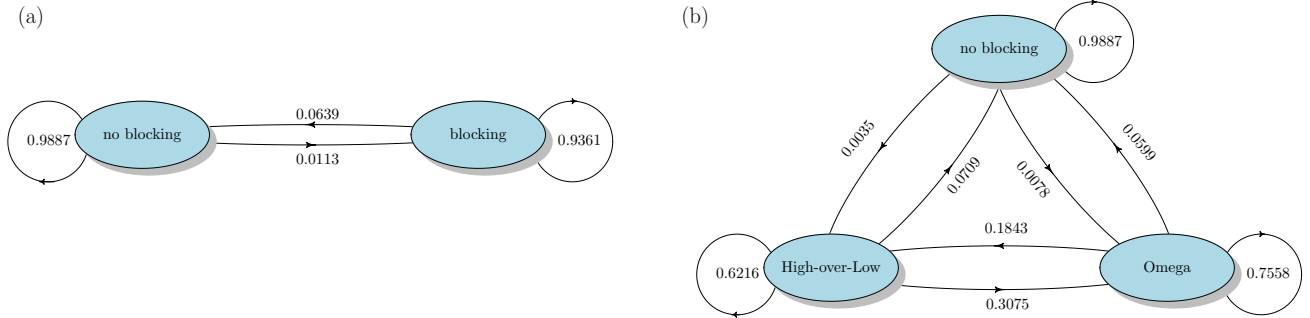
Figure 10 shows the temporal evolution of (a) *High-over-Low* and (b) *Omega* blocking patterns in the time period 1990 to 2019 broken down to the seasons. For *High-over-Low* blocks, the Euro-Atlantic region shows for this 30-year period a

350   decrease/slight decrease in winter (DJF)/summer (JJA) and an increase/slight increase in spring (MAM)/autumn (SON) (see Fig. 10a). At the same time, the probability for *Omega* blocks increases strongly in the summer months from $p \approx 0.04$ in 1990 to $p \approx 0.08$ in 2019 and also pronounced from $p \approx 0.085$ in 1990 to $p \approx 0.115$ in 2019 in winter and spring (see Fig. 10b). Only the *Omega* blocks in autumn (SON) decrease from $p \approx 0.12$ to $p \approx 0.085$ over 30 years. Interestingly, the blocked summer High-over-Lows start with the same probability as the *Omega* blocks in the 1990s. However, while probability increases

Figure 11. Blocking probability over time for individual month (Eq. 20) for *High-over-Low* (solid) and *Omega* (dashed) blocking. Shadings show 95% confidence intervals. (a) winter (DJF) (b) spring (MAM) (c) summer (JJA) and (d) autumn (SON) in the Euro-Atlantic region $(40° W - 30° E)$.

355 strongly for *Omega* blocks, it shows only a very slight increase for *High-over-Low*s. Hence, the observed, general increase in summer blocking probability (Fig. 7b) can be attributed to an increase in *Omega* block patterns. This increase occurs in all three summer months, but stronger in June and August (see Fig. 8c).

The monthly development of the *High-over-Low* and *Omega* blocking are also shown in Fig. 11. For the winter season, the increase is marked by *Omega* blocks, especially in months February and January. The *High-over-Low* blocking shows more an

360 decrease and only a slight increase in February (see Fig. 11a). In spring, the frequencies for *High-over-Low* blocking remain largely constant, with only a slight increase in March. *Omega* blocks therefore play a greater role in the development of these frequencies here as well. The highest change is in March (see Fig. 11b). In the summer months the change is not as pronounced than in the other seasons and is again mainly dominated by *Omega* blocks (see Fig. 11c). In autumn there is virtually no change in the blocking state (see Fig. 7). An analysis of the individual months shows a slight increase in the probabilities in November.

(a)

(b)

Figure 12. Graph representation of the transition matrix estimate for a Markov process (a) with two states (Eq. 11) and (b) with three states (Eq. 12) in the Euro-Atlantic region ($40° W - 30° E$).

The other two months, however, show a decrease. All in all, this balances itself out. The change of the *High-over-Low* blocking, however, shows a different change. There is a slight increase in September. This seems to be balanced by a decrease in *Omega* blocks (see Fig. 11d).

4.3 Transition probabilities

We conceive the dynamics between different blocking and no-blocking states as a stochastic process with Markov properties (see Section 3.6) and give transition probabilities for the two- and three-states model with stationary and non-stationary assumptions in the following.

4.3.1 Stationary transition probabilities of two- and of three-state models

Assuming stationary transition probabilities, we can estimate transition matrices for the two- and of three-state models. Figure 12 shows the transition probabilities of the two-state model with *no blocking* and *blocking* (left) and the three-state model (*no blocking*, *High-over-Low* and *Omega block*) (right).

We call the probability to remain in one state *stability* or persistence and the transition from *no blocking* to a *blocking* (*High-over-Low* or *Omega*) *onset*; the opposite direction is called *offset*. For both models, persistence (probability to remain in one state) of either state is higher than transition probabilities to other states; particularly high is the persistence of the no-blocking state. The latter is due to the fact that there are considerably more time steps without blocking than blocked states. But if blocking occurs, the probability to remain in this condition is high, too.

For the three-states model, the onset probability for an *Omega* blocking is higher than that for a *High-over-Low* blocking. Both values are small compared to the persistence defined above. This is consistent with the fact that onsets are less frequent. With this model, we obtain that *Omega* blocking is more stable than *High-over-Low* ($Pr\{Y_t = \Omega \mid Y_{t-1} = \Omega\} > Pr\{Y_t = HoL \mid Y_{t-1} = HoL\}$ and *High-over-Low* is more likely to evolve into *Omega* than vice versa. The decay of an *Omega* block to a no-blocking state is also less likely than the decay of a *High-over-Low* block ($Pr\{Y_t = nB \mid Y_{t-1} = \Omega\} > Pr\{nB \mid Y_{t-1} =$

$HoL\}$). This means that in the area of a *High-over-Low* block, another low-pressure system moves in and the structure shifts to an *Omega* blocking. This occurs more often than that a low pressure system moves out of the structure and thus turns the system into a *High-over-Low* pattern.

4.3.2 Non-stationary transition probabilities of two- and of three-state models

390 Of particular interest is a potential change in transition probabilities during the study period 1990 to 2019. To this end, we describe the change in transition probabilities using logistic regression with year (and season) as interacting terms in the predictor as given in Eq. 13 (Eq. 21), see also Sec. 3.6. Figure 13 shows the time varying transition probabilities for the two-state model arranged analogously to the transition matrix (Eq. 11). The shadings give 95 % confidence intervals.

For both, onset ($p_{B|nB}$) and offset ($p_{nB|B}$), the transition probability increases slightly, however not significant. Breaking
395 this down into seasons with another interaction effect

$$\mathrm{logit}(Pr\{Y_t = B \mid Y_{t-1}\}) \sim Y_{t-1} * \mathrm{Year} * \mathrm{Seas}, \tag{21}$$
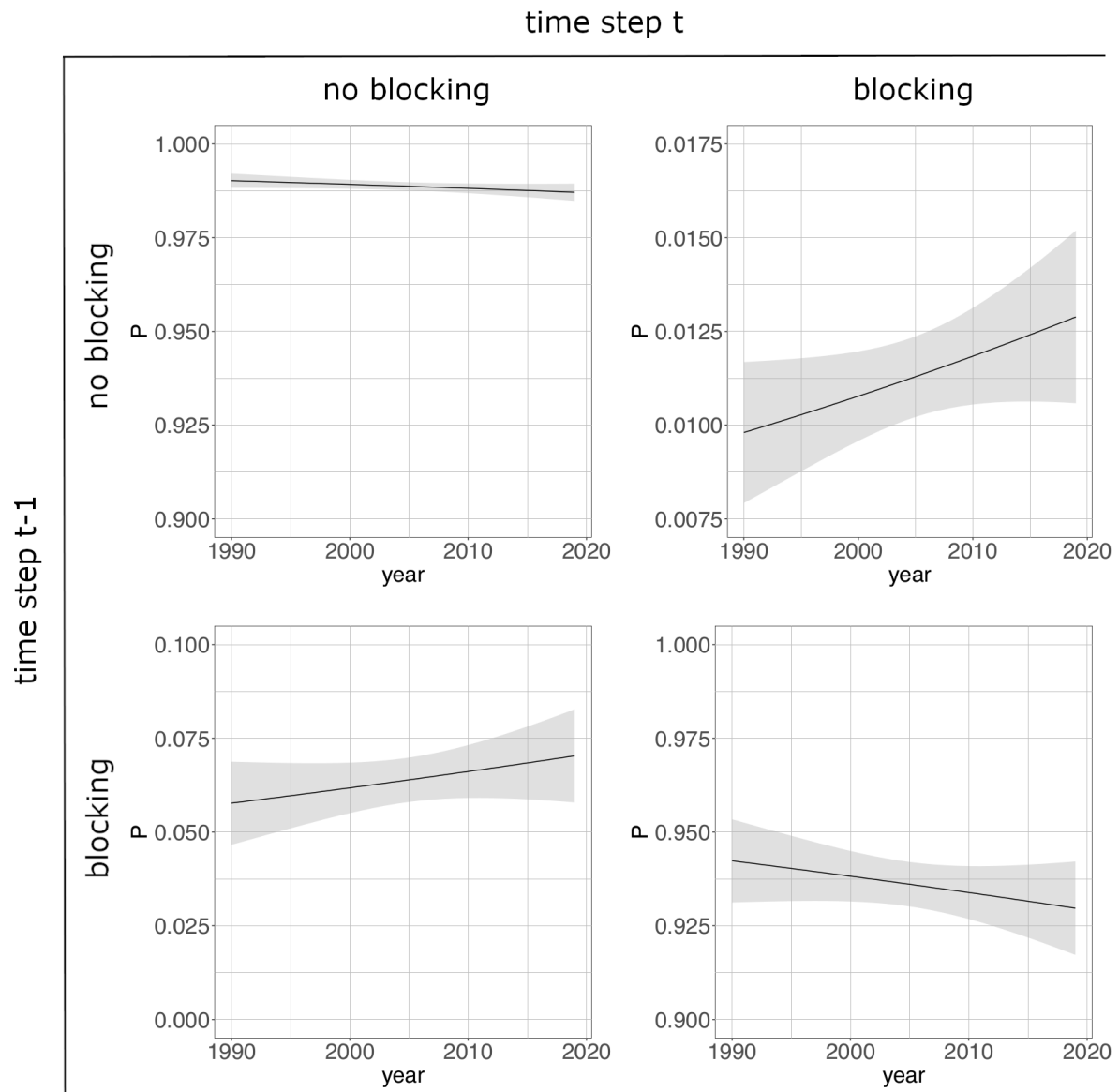
we find the strongest temporal change in summer (JJA), see Fig. 14. However, only changes of persistence of no blocking and the onset are significantly different from the horizontal line. The onset probability increases and the probability of remaining in the no-blocking state decrease. Along with the increasing offset probability (not significant) and the decreasing persistence
400 of blocking, we can conclude that the frequency of blocking increase while the persistence decreases.

Fig. 15 shows the time varying transition probabilities of a Markov model with three states (Eq. 12), estimated using multinomial regression.
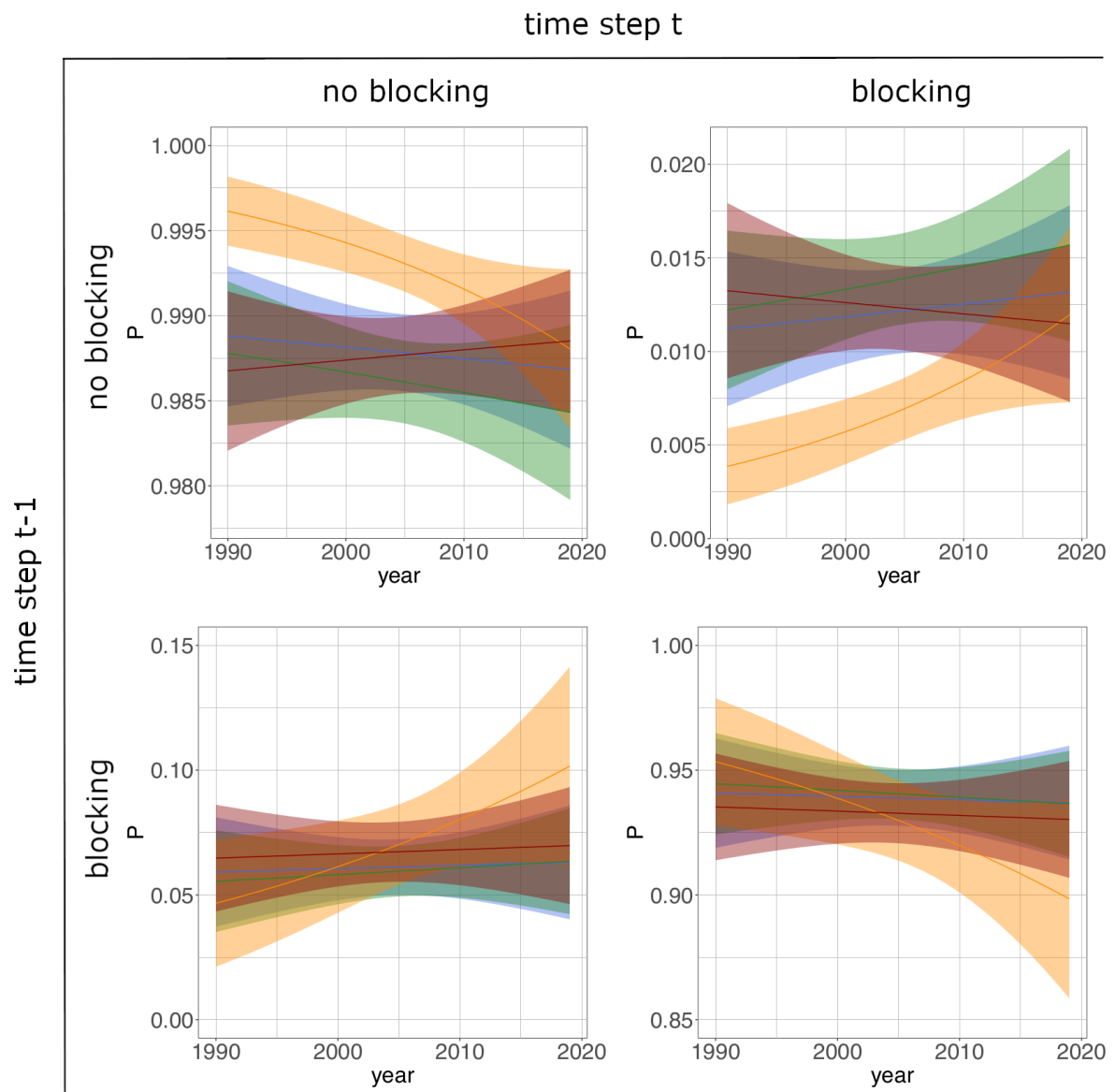
$$\ln\left(\frac{Pr\{Y_t = HoL\} \mid Pr\{Y_{t-1}\}}{Pr\{Y_t = nB \mid Y_{t-1}\}}\right) \sim Y_{t-1} * \mathrm{Year}, \qquad \ln\left(\frac{Pr\{Y_t = \Omega\} \mid Pr\{Y_{t-1}\}}{Pr\{Y_t = nB \mid Y_{t-1}\}}\right) \sim Y_{t-1} * \mathrm{Year} \tag{22}$$

Similar to the two-state model, the probability for remaining in a no blocking state slightly (but significantly) decreases and
405 the onset probability for an *Omega* block slightly (and significantly) increases. Note also the decrease of transition probability from *Omega* to *High-over-Low* $p_{HoL|\Omega}$ which is compensated by an increase in persistence of *Omega* $p_{\Omega|\Omega}$ and an increase of offset probability from *Omega* blocking $p_{\Omega|nB}$ (all three not significant). We can thus refine the impression from the two-state model: blocking are more frequent and those are predominantly *Omega*, which become more stable and do less likely evolve into *High-over-Low*s.
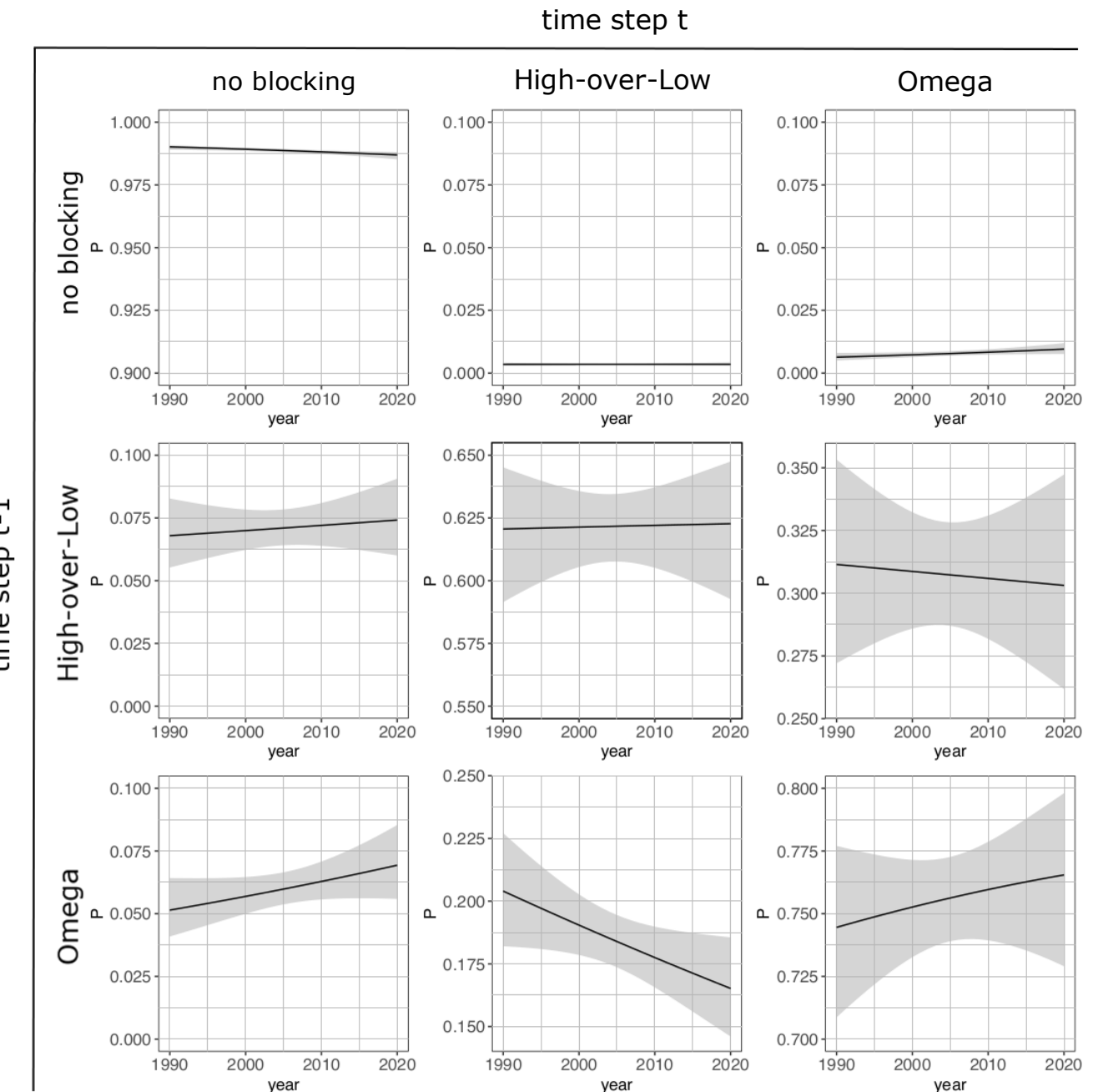
410 Breaking this down into seasons by adding another interaction effect (Eq. 14 and 15), we obtain Fig. 16. The largest temporal changes can again be observed in the summer months. The first row shows an increase in the onset probability for *Omega* blocks in summer while the probability of remaining in a no blocking state decreases. The last row shows that *Omega* blocks become slightly more stable in summer towards the end of the study period and becomes less likely to evolve into a *High-over-Low* (both not significant). Changes in transition probabilities for *High-over-Low* blocks are in the second row of
415 Fig.16: A decrease in persistence in summer and an increase in stability in the other seasons. The transition probability to *Omega* blocks increase strongly in summer and slightly in winter and decrease in the transition seasons (all not significant). This confirms again the previously gained impressions: *Omega* blocks become more frequent and stable in summer and the
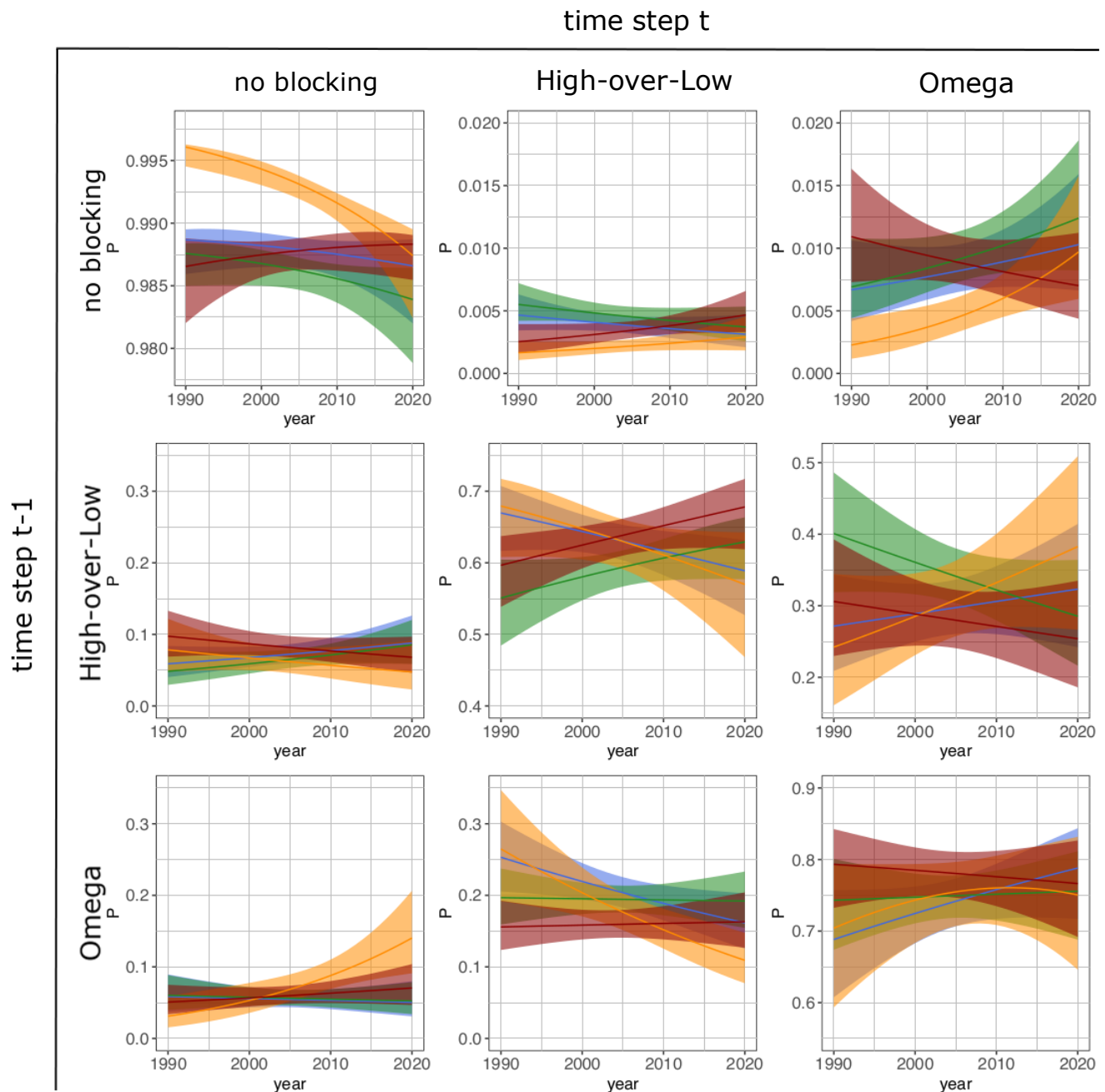
Figure 13. Transition probabilities analogous to the matrix of a two-state Markov process (Eq. 11) as a function of years (Eq. 13) in the Euro-Atlantic region ($40°\,W - 30°\,E$). Top left: $p_{nB|nB} = Pr\{Y_t = nB \mid Y_{t-1} = nB\}$, top right: $p_{B|nB} = Pr\{Y_t = B \mid Y_{t-1} = nB\}$, bottom left: $p_{nB|B} = Pr\{Y_t = nB \mid Y_{t-1} = B\}$ and bottom right: $p_{B|B} = Pr\{Y_t = B \mid Y_{t-1} = B\}$. Shadings show 95 % confidence intervals.

Figure 14. Transition probabilities analogous to the matrix of a two-state Markov process (Eq. 11) as a function of years for individual seasons (Eq. 21) in the Euro-Atlantic region ($40° W - 30° E$). Top left: $p_{nB|nB}$, top right: $p_{B|nB}$, bottom left: $p_{nB|B}$ and bottom right: $p_{B|B}$. Shadings show 95 % confidence intervals.

Figure 15. Transition probabilities analogous to the matrix of a three-state Markov process (Eq. 12) as a function of years (Eq. 22) in the Euro-Atlantic region ($40° W - 30° E$). Top left: $p_{nB|nB}$, top center: $p_{HoL|nB}$ top right: $p_{\Omega|nB}$, middle left: $p_{nB|HoL}$, middle center: $p_{HoL|HoL}$ middle right: $p_{\Omega|HoL}$, bottom left: $p_{nB|\Omega}$, bottom center: $p_{HoL|\Omega}$ and bottom right: $p_{\Omega|\Omega}$. Shadings show 95 % confidence intervals.

Figure 16. Transition probabilities analogous to the matrix of a three-state Markov process (Eq. 12) as a function of years for individual seasons (Eq. 14 and Eq. 15) in the Euro-Atlantic region ($40° W - 30° E$). Panels are ordered analogously to Fig. 15, season is color coded. Shadings show 95 % confidence intervals.

transition probability of *High-over-Low* to *Omega* decreases in summer. The persistence of *High-over-Low* increase over the years in the transition seasons and become less likely to evolve into an *Omega*, although these changes are not significant.

5 Discussion

In this work, we analyse onset, offset and transition probabilities of atmospheric blocking. As novel aspects, we use a Markov model and we distinguish between the two blocking types *High-over-Low* and *Omega* blocking. The general investigations of the duration and number of blocking during the past 30 years as well as the time evolution of the relative frequency of blocking according to its seasonal distribution and the annual evolution of blocks in Figures 5, 6, 7 and 9 are evaluated for the region $90°\,W - 90°\,E$ and also for the Euro-Atlantic sector $40°\,W - 30°\,E$. To gain further insight into the temporal development of the relative frequency of blocking of the individual months, see Fig. 8, and to compare the different blocking types with respect to their seasonal development in Fig. 10 we concentrated on the Euro-Atlantic region. We also calculate the transition probabilities of two states (*no blocking, blocking*) in Fig. 12a and of three states (*no blocking, High-over-Low, Omega block*) in Fig. 12b. The evolution of these transition probabilities in the temporal and seasonal development for the Euro-Atlantic region is as well shown for two states (see Fig. 13 and 14) and for three states (see Fig. 15 and 16).

Regarding the past 30 years, Fig. 6 does not show a significant trend of the number of blocking events in the Euro-Atlantic sector. But the mean duration of a blocked system (*High-over-Low* or *Omega*) did slightly increase during the past 30 years by about 2 time steps (≈ 12 h) in both inspected regions. However in the larger domain (90°W-90°E), the maximum duration of the blocking events increases strongly by about 2.1 days ($\approx$8 to 9 time steps) over the 30 year period. This increase can be attributed to the blocking events that occur over (western) Russia. Splitting the evolution of the time of the relative frequency of blocking into seasons, as shown in Fig. 7, an increase of the probability of blocking in the spring and in the summer months can be recognized. In Fig. 9 the seasonal frequency for *High-over-Low* and for *Omega* blocks in the Euro-Atlantic region are shown. These figures indicate an increase of the *Omega* blocking events in winter, spring and summer. We also find that the occurrence probability of an *Omega* blocking is higher than that of a *High-over-Low*. Moreover, over the 30 year period we observe a strong increase of blocked periods in February and March (Fig. 8). These late winter/early spring blocks can have a significant impact on the vegetation and on agriculture in general since they are often connected to temperature extremes. E.g. Brunner et al. (2017) found a strong link between cold spell days in February and co-occurrence of blocking, and a link between warm spell days and blocking in late spring, however, they found "no apparent trend in the number of blocked days".

We newly introduced the blocking type decision method, that identifies *High-over-Low* and *Omega* patterns for each blocked time step, separately. These blocked time steps are initially identified with the help of the instantaneous blocking longitude (IBL) method after Tibaldi and Molteni (1990) (see also Richling et al., 2015). However, the identification algorithm (Step 1-4, sections 3, see also Fig. 2) is based on many assumptions and not flawless. Hence, we want to discuss some possible error sources here. The IBL method is a one-dimensional method. Although we applied a seasonally varying reference latitude, a one-dimensional method might have problems in detecting blocked situations properly. Especially, the thresholds of northern and southern geopotential height gradients are fixed values and applied for the whole year. This might explain why there

are fewer blocks detected in summer. See also e.g. Scherrer et al. (2006), who show that the frequency of blocks is strongly

dependent on the reference latitude. Moreover, the choice of the investigated domain can have an impact on the results, see e.g.

Fig. 7. We also note that the data assimilation techniques as well as the amount of observational data assimilated did change

over the years, which can lead to slightly inhomogeneous data. This might further obscure real trends from artificial ones (Sterl,

455   2004). Since our study regions are in the northern hemispheric mid-latitudes and our period lies in the post-satellite era, we

expect the data to be relative homogeneous. We also choose five days (=20 time steps) as a minimum duration for our definition

of blocking in the larger domain. Although we made a subset of the larger domain and the length of stay within the smaller

Euro-Atlantic sector can be smaller than 5 days, the minimum lifetime of the associated block period is still 5 days. However,

changing this minimum duration leads to deviations of the results.

460   Investigating the blocking identification methods based on the vertically averaged potential vorticity anomaly (Schwierz

et al., 2004), the geopotential height anomaly (Dole and Gordon, 1983), and geopotential height gradient after Tibaldi and

Molteni (1990) that is applied here, Pinheiro et al. (2019) found that *each of the three algorithms produce distinct regional and*

seasonal differences in their overall global blocking climatology. Moreover, the decision between *High-over-Low* and *Omega*

blocking types is based on a comparison of the vortex field south of the high center. The vortex field is inspected in a box with

465   a width of 25 degrees longitudes directly below the high and compared to the two neighboring boxes (see Fig. 3). A change in

the box width obviously can affect the percentage of identified *High-over-Lows* vs. *Omega* blocks. In our setting, the method

identifies about 2/3 of all blocking as *Omega* types. Furthermore, changing the region of interest (Step 4 in Section 3) can

lead to different results than previous works. A major benefit of this approach based on the kinematic vorticity number is the

identification and location of each single vortex – the high pressure area as well as the one or two low pressure areas – forming

470   the *High-over-Low*, respectively the *Omega* block.

Most blocks occur in spring and in autumn (see Fig. 9). In summer, especially in August, the probability of blocking is

rather small. This can be explained by the variation of the pressure anomalies. In spring and autumn the amplitudes of the

pressure anomalies are larger than in summer (see, e.g. Wallace et al., 1993). Therefore, the high and low pressure systems

are more distinct and can last longer. In Fig. 7 the blocking occurrence probabilities split to seasons are illustrated, where

475   the low probability of blocking in the summer months in the Euro-Atlantic sector is clearly recognizable. Tyrlis and Hoskins

(2008) and Brunner et al. (2017) show similar results. But as shown in Fig. 9 the number of blocks slightly increase. Therefore,

occurrences of exceptional droughts, that were experienced 2018 and 2019 in central Europe (Hari et al., 2020) are possible.

As a novel aspect, we analyse the transition probabilities of the blocked weather systems with Markov models. First, we

considered a Markov process with the two states *no blocking* and *blocking*. Fig. 12a shows that in the Euro-Atlantic region,

480   the probability that a blocking remains blocked is 0.94. The probability of the onset, i.e. the transition probability from the

state *no blocking* to the state *blocking*, is much lower (about 1%) than the offset probability (about 6%), because there are

more time steps unblocked than blocked. In comparison, Spekat et al. (1983) found daily transition probabilities for the onset

of a meridional weather regime of 8% (zonal→meridional) to 11% (mixed state→meridional) and high probabilities to stay

within the same weather regime (between 0.81 and 0.86). Their offset probabilities range from 5% (meridional→zonal) to

485   9% (meridional→mixed state). However, their mixed state can contain blocking as well and the meridional state can also be

composed of an extended large-scale trough. Nevertheless, their onset values are comparable to our results if we downscale the 6-hourly data to daily time steps. Moreover, we can confirm that the probability is higher to remain within the same state. A more detailed comparison is complicated since the definition of the atmospheric states differs from the one we use. While Spekat et al. (1983) uses a large-scale weather regime classification, our method is based on the identification of the blocking

490   pattern itself and is rather event-based. Fig. 13 and Fig. 14 show a temporal increase of transitions from the state *no blocking* to *blocking*.

In Fig. 12b, we additionally consider the type of the block. Here, we differentiate the three states by *no blocking*, *High-over-Low* and *Omega* block. Fig. 12b shows that the *Omega* block is more persistent than the *High-over-Low* system. Moreover, the formation or onset probability of an *Omega* block is higher than that of a *High-over-Low* blocking. Furthermore, the transition

495   probability from the *High-over-Low* state to the *Omega* block is 0.3, whereas the transition probability from a *High-over-Low* to an *Omega* block is considerably smaller (0.18). Analysing composites of the blocking onset in the time period June to August, Drouard and Woollings (2018) found that Western- and Central Europe are dominated by a *High-over-Low* pattern while they found an *Omega* pattern for East Europe east of $35° E$. However, since our identification and regions differ, we can neither confirm nor deny this observation. Furthermore, we observe a positive trend regarding the onset of *Omega* blocks over the

500   past 30 years (see Fig. 15). Moreover, Lucarini et al. (2016) finds that blocking periods are characterized by higher instability than unblocked flows. This might also justify the occurrence of blocking type changes from *High-over-Low* to *Omega* and vice versa.

To answer the question if the transition probabilities of the three states have changed in the time period 1990-2019 in the Euro-Atlantic region, we show the transition probabilities between the states *no blocking*, *High-over-Low* and *Omega block*

505   in Fig. 15 and Fig. 16. In summary, it has been shown that the greatest changes occurred between 1990 and 2019 for *Omega* blocking. The transition probabilities for onset and offset have slightly increased, the conversion from a *High-over-Low* to an *Omega* block and from an *Omega* to a *High-over-Low* blocking has decreased and it is shown that *Omega* blocks remain in their state for more time steps.

6   Conclusion

510   Using logistic regression and Markov model, we investigate onset, offset and transition probabilities of atmospheric blocking. Evaluating the NCEP-DOE Reanalysis 2 data set for the time period 1990-2019, we show the temporal evolution of the relative frequency of blocking in the Euro-Atlantic sector (40°W-30°E) and for half of the northern hemisphere (90°W-90°E). First, we use logistic regression to investigate the temporal development of blocking probabilities depending on years, seasons and months. For both regions, we observe no significant increase in the yearly blocking frequency over the 30 year period. But, we

515   find large increases in blocking probability over the 30 year period for February and March that are compensated by decreasing probabilities in December and autumn. We observe a steady, but slight increase for the summer months, too. This increasing probability can mainly be attributed to an increase in *Omega* blocking.

Regarding the proportion of *Omega* and *High-over-Low* blocks with respect to all observed blocks. In general we found that 2/3 of all identified blocks are *Omega* blocks. However, we find some interesting developments for specific months over the

520   30 years (cf. Fig. 11). While in July the proportion of *Omega* blocks is only about 25% of all observed blocks in 1990, we find on the one hand an increase in overall probability for blocking as well as a higher proportion towards the end of the study period. In 2019, the *Omega* blocks pose about 80% of all blocking. Interestingly this relation is reversed in September where the *High-over-Low*s constitute about 20% of all blocking in 1990 vs. about 55% in 2019. It is not clear, why there is a change in the distribution of blocking types. Future studies are challenged to look for changes in e.g. dynamical processes in this time

525   period that might cause this differences.

Second, we use the Markov model to calculate transition probabilities of the different blocking types *High-over-Low* and *Omega* blocking and of the state *no blocking*. We show that *Omega* blocking is more likely to occur and more persistent than the *High-over-Low* blocking pattern. Regarding the seasons over the 30 year period, we found the largest changes in transition probabilities in the summer season, where the transition probability to *Omega* blocks increase strongly, while the

530   *unblocked* state becomes less probable. Hence, *Omega* blocks become more frequent and stable in summer. Moreover, we observe a higher probability for the transition from *High-over-Low* to *Omega* blocks in the summer season towards the end of the study period (cf. Fig. 16). This confirms the impression that blocking in summer become more prominent in recent years over the European continents. Additionally, we show that this increase in summer blocking is explained by an increase in *Omega* blocking patterns. In general, we find no significant trends (except for the summer months) in the transition of the

535   blocking states, which is in accordance with e.g. Wiedenmann et al. (2002) or Tyrlis and Hoskins (2008).

In future studies, the relation of on- and offset of blocking to different parameters as the NAO, the temperature, or the wind shear will further be investigated. For further investigations of atmospheric blocking, the authors suggest to use the kinematic vorticity number to search for the high pressure area (after Schielicke et al., 2016) and then follow the steps 2-6 as suggested in the flow chart in Fig. 2. Moreover, since this method locally identifies the high and the low pressure areas, it can further be

540   used for a statistical evaluation of extreme events caused by the high *and* the low(s), e.g. droughts and floods.

We conclude, that the use of Markov models with two and three possible states as well as the split into different blocking types gives valuable insight into the development of atmospheric blocking.

Author contributions. A.M., P.N. and H.R. designed the study. C.D. did the statistical analysis and visualised the results, mainly at the FU Berlin. L.S. wrote and adapted the trapezoid method and blocking type decision method. H.R. and C.D. wrote the statistical chapters and

545   discussed the related results. C.D., A.M. and L.S. continuously wrote on the paper draft and discussed the results. All authors discussed and finalised together the paper.

Competing interests. The authors declare that no competing interests are present.

Acknowledgements. We thank I. Kröner for critical discussions and reading the manuscript. This research has been partially funded by Deutsche Forschungsgemeinschaft (DFG) through grant CRC 1114 'Scaling Cascades in Complex Systems, Project Number 235221301, Projects A01 'Coupling a multiscale stochastic precipitation model to large scale atmospheric flow dynamics' and C06 'Multiscale structure of atmospheric vortices'.

550

References

Altenhoff, A. M., Martius, O., Croci-Maspoli, M., Schwierz, C., and Davies, H. C.: Linkage of atmospheric blocks and synoptic-scale Rossby waves: a climatological analysis, Tellus A, 60, 1053–1063, https://doi.org/10.1111/j.1600-0870.2008.00354.x, 2008.

555 Aref, H.: Motion of three vortices, Physical Fluids, 22, 1979.

Baclawski, K.: Introduction to probability with R, Chapman & Hall/CRC Texts in statistical science, 2008.

Barnes, E. A., Slingo, J., and Woollings, T.: A methodology for the comparison of blocking climatologies across indices, models and climate scenarios, Climate Dynamics, 38, 2467–2481, https://doi.org/10.1007/s00382-011-1243-6, 2011.

Barriopedro, D., García-Herrera, R., Lupo, A. R., and Hernández, E.: A climatology of Northern Hemisphere blocking, Journal of Climate,

560 19, 1042–1063, https://doi.org/10.1175/JCLI3678.1, 2006.

Barriopedro, D., García-Herrera, R., and Trigo, R.: Application of blocking diagnosis methods to general circulation models. Part I: A novel detection scheme, Climate dynamics, http://link.springer.com/article/10.1007/s00382-010-0767-5, 2010.

Berrisford, P., Hoskins, B. J., and Tyrlis, E.: Blocking and Rossby Wave Breaking on the Dynamical Tropopause in the Southern Hemisphere, Journal of the Atmospheric Sciences, 64, 2881–2898, https://doi.org/10.1175/JAS3984.1, 2007.

565 Bissolli, P., Deutschländer, T., Imbery, F., Haeseler, S., Lefebvre, C., Blahak, J., Fleckenstein, R., Breyer, J., Rocek, M., Kreienkamp, F., Rösner, S., and Schreiber, K.-J.: Hitzewelle Juli 2019 in Westeuropa – neuer nationaler Rekord in Deutschland, https://www.dwd. de/DE/leistungen/besondereereignisse/temperatur/20190801_hitzerekord_juli2019.pdf?__blob=publicationFile&v=3, Deutscher Wetterdienst, Abteilung Klimaüberwachung. Press release (in German), 1 Aug 2019 (last access: 31 Aug 2020), 2019.

Bott, A.: Synoptische Meteorologie, Springer Berlin Heidelberg, https://doi.org/10.1007/978-3-642-25122-1, 2012.

570 Brunner, L., Hegerl, G. C., and Steiner, A. K.: Connecting atmospheric blocking to European temperature extremes in spring, Journal of Climate, 30, 585–594, 2017.

Brunner, L., Schaller, N., Anstey, J., Sillmann, J., and Steiner, A. K.: Dependence of present and future European temperature extremes on the location of atmospheric blocking, Geophysical research letters, 45, 6311–6320, 2018.

Davini, P., Cagnazzo, C., Gualdi, S., and Navarra, A.: Bidimensional diagnostics, variability, and trends of Northern Hemisphere blocking,

575 Journal of Climate, 25, 6496–6509, 2012.

Deutscher Wetterdienst: The weather in Germany in July 2019, https://www.dwd.de/EN/press/press_release/EN/2019/20190730_the_ weather_in_germany_in_july_2019.pdf?__blob=publicationFile&v=2, press release, 30 July 2019 (last access: 31 Aug 2020), 2019.

Dobson, A. J. and Barnett, A. G.: An introduction to generalized linear models, Third Edition, Texts in Statistical Science, Chapman & Hall, 2008.

580 Dole, R. M. and Gordon, N. D.: Persistent anomalies of the extratropical northern hemisphere wintertime circulation: Geographical distribution and regional persistence characteristics, Monthly Weather Review, 111, 1567–1586, 1983.

Drouard, M. and Woollings, T.: Contrasting mechanisms of summer blocking over western Eurasia, Geophysical Research Letters, 45, 12–040, 2018.

Egger, J.: The blocking transition, in: Irreversible phenomena and dynamical systems analysis in geosciences, edited by Nicolis, C. and

585 Nicolis, G., pp. 181–197, Springer Netherlands, Dordrecht, https://doi.org/10.1007/978-94-009-4778-8_10, 1987.

Ferranti, L., Corti, S., and Janousek, M.: Flow-dependent verification of the ECMWF ensemble over the Euro-Atlantic sector, Quarterly Journal of the Royal Meteorological Society, 141, 916–924, 2015.

Freva: Freie Universität Berlin evaluation system (Freva), https://freva.met.fu-berlin.de/, accessed: 2020-09-10, 2017.

Gottwald, G. A., Crommelin, D. T., and Franzke, C. L. E.: Stochastic climate theory, arXiv, (last access: 31 Aug 2020), 2016.

590 Grewal, J. K., Krzywinski, M., and Altman, N.: Markov models – Markov chains, Nature Methods, 16, 663–664, https://doi.org/10.1038/s41592-019-0476-x, 2019.

Hari, V., Rakovec, O., Markonis, Y., Hanel, M., and Kumar, R.: Increased future occurrences of the exceptional 2018–2019 Central European drought under global warming, Scientific Reports, 10, 1–10, 2020.

Helmholtz, H.: Über Integrale der hydrodynamischen Gleichungen welche den Wirbelbewegungen entsprechen, Journal für die reine und

595 angewandte Mathematik, 55, 25–55, 1858.

Henley, J., Chrisafis, A., and Jones, S.: France records all-time highest temperature of 45.9C, The Guardian, 28 Jun 2019 (last access: 31 Aug 2020), 2019.

Hirt, M., Schielicke, L., Müller, A., and Névir, P.: Statistics and dynamics of blockings with a point vortex model, Tellus A: Dynamic Meteorology and Oceanography, 70, 1–20, 2018.

600 Hong, C.-C., Hsu, H.-H., Lin, N.-H., and Chiu, H.: Roles of European blocking and tropical-extratropical interaction in the 2010 Pakistan flooding, Geophysical Research Letters, 38, 2011.

Kanamitsu, M., Ebisuzaki, W., Woollen, J., Yang, S.-K., Hnilo, J., Fiorino, M., and Potter, G.: Ncep–doe amip-ii reanalysis (r-2), Bulletin of the American Meteorological Society, 83, 1631–1644, 2002.

Kimoto, M. and Ghil, M.: Multiple flow regimes in the Northern Hemisphere winter. Part II: Sectorial regimes and preferred transitions,

605 Journal of the atmospheric sciences, 50, 2645–2673, 1993.

Kuhlbrodt, T. and Névir, P.: Low-order point vortex models of atmospheric blocking, Meteorology and Atmospheric Physics, 73, 127–138, 2000.

Lucarini, V., Freitas, A. C. M., Nicol, M., Freitas, J. M., Todd, M., Faranda, D., Kuna, T., Hollande, M., and Vaienti, S.: Extremes and recurrence in dynamical systems, Wiley, 2016.

610 Matlab: MATLAB version 9.0.0.341360 (R2016a), The MathWorks Inc., Natick, Massachusetts, 2016.

McCullagh, P. and Nelder, J. A.: Generalized Linear Models 2nd edition, London, UK, 1989.

Mohr, S., Wilhelm, J., Wandel, J., Kunz, M., Portmann, R., Punge, H. J., Schmidberger, M., Quinting, J. F., and Grams, C. M.: The role of large-scale dynamics in an exceptional sequence of severe thunderstorms in Europe May–June 2018, Weather and Climate Dynamics, 1, 325–348, https://doi.org/10.5194/wcd-1-325-2020, 2020.

615 Müller, A. and Névir, P.: A geometric application of Nambu mechanics: the motion of three point vortices in the plane, Journal of Physics A: Mathematical and Theoretical, 47, 105 201, 2014.

Müller, A., Névir, P., Schielicke, L., Hirt, M., Pueltz, J., and Sonntag, I.: Applications of point vortex equilibria: blocking events and the stability of the polar vortex, Tellus A, 67, https://doi.org/10.3402/tellusa.v67.29184, 2015.

Newton, P. K.: The N-Vortex Problem: Analytical Techniques, Springer-Verlag, 2001.

620 Obukhov, A., Kurganskii, M., and Tatarskaia, M.: Dynamic conditions for the origin of drought and other large-scale weather anomalies, Meteorologiia i Gidrologiia, pp. 5–13, 1984.

Pelly, J. L. and Hoskins, B. J.: A new perspective on blocking, Journal of the atmospheric sciences, 60, 743–755, 2003.

Pfahl, S. and Wernli, H.: Quantifying the relevance of atmospheric blocking for co-located temperature extremes in the Northern Hemisphere on (sub-) daily time scales, Geophysical Research Letters, 39, 2012.

625 Pinheiro, M., Ullrich, P., and Grotjahn, R.: Atmospheric blocking and intercomparison of objective detection methods: flow field characteristics, Climate dynamics, 53, 4189–4216, 2019.

R Core Team: R: A language and environment for statistical computing, R Foundation for Statistical Computing, Vienna, Austria, https://www.R-project.org/, 2018.

Rex, D. F.: Blocking action in the middle troposphere and its effect upon regional climate: Part I. An aerological study of blocking action, Tellus, 2, 196–211, 1950.

Richling, A., Kadow, C., Illing, S., and Kunst, O.: Freie Universität Berlin evaluation system (Freva) - Blocking, https://freva.met.fu-berlin.de/about/blocking/, (Documentation of the blocking plugin), Accessed: 2020-09-10, 2015.

Scherrer, S. C., Croci-Maspoli, M., Schwierz, C., and Appenzeller, C.: Two-dimensional indices of atmospheric blocking and their statistical relationship with winter climate patterns in the Euro-Atlantic region, International Journal of Climatology: A Journal of the Royal Meteorological Society, 26, 233–249, 2006.

Schielicke, L.: Scale-dependent identification and statistical analysis of atmospheric vortex structures in theory, model and observation, Ph.D. thesis, Freie Universität Berlin, Berlin, Germany, 2017.

Schielicke, L., Névir, P., and Ulbrich, U.: Kinematic vorticity number – a tool for estimating vortex sizes and circulations, Tellus A, 68, https://doi.org/10.3402/tellusa.v68.29464, 2016.

Schwierz, C., Croci-Maspoli, M., and Davies, H.: Perspicacious indicators of atmospheric blocking, Geophysical research letters, 31, 2004.

Spekat, A., Heller-Schulze, B., and Lutz, M.: Über Großwetterlagen und Markov-Ketten, Meteorologische Rundschau, 36, 243–248, in German, 1983.

Sterl, A.: On the (in) homogeneity of reanalysis products, Journal of Climate, 17, 3866–3873, 2004.

Tibaldi, S. and Molteni, F.: On the operational predictability of blocking, Tellus A, 42, 343–365, https://doi.org/10.1034/j.1600-0870.1990.t01-2-00003.x, 1990.

Truesdell, C.: Two measures of vorticity, Indiana Univ. Math. J., 2, 173–217, 1953.

Truesdell, C.: The kinematics of vorticity, Indiana University Press, Bloomington, Indiana, 1954.

Tung, K. K. and Lindzen, R.: A theory of stationary long waves. Part I: A simple theory of blocking, Monthly Weather Review, 107, 714–734, 1979.

Tyrlis, E. and Hoskins, B. J.: Aspects of a northern hemisphere atmospheric blocking Climatology, Journal of the Atmospheric Sciences, 65, 1638–1652, https://doi.org/10.1175/2007JAS2337.1, 2008.

Vautard, R., Mo, K. C., and Ghil, M.: Statistical significance test for transition matrices of atmospheric Markov chains, Journal of the atmospheric sciences, 47, 1926–1931, 1990.

Wallace, J. M., Zhang, Y., and Lau, K.-H.: Structure and seasonality of interannual and interdecadal variability of the geopotential height and temperature fields in the Northern Hemisphere troposphere, Journal of Climate, 6, 2063–2082, 1993.

Werner, P. C. and Gerstengarbe, F.-W.: Katalog der Grosswetterlagen Europas (1881-2009) nach Paul Hess und Helmut Brezoswky, 7. verbesserte und ergänzte Aauflage, PIK Report, No. 119, Tech. rep., Potsdam-Institut für Klimafolgenforschung (PIK), https://www.pik-potsdam.de/research/publications/pikreports/.files/pr119.pdf, 2010.

Wiedenmann, J. M., Lupo, A. R., Mokhov, I. I., and Tikhonova, E. A.: The climatology of blocking anticyclones for the Northern and Southern Hemispheres: Block intensity as a diagnostic, Journal of Climate, 15, 3459–3473, 2002.

Wilks, D. S.: Statistical methods in the atmospheric sciences, vol. 100 of *International geophysics series*, Academic Press, 3 edn., 2011.

Woollings, T., Barriopedro, D., Methven, J., Son, S.-W., Martius, O., Harvey, B., Sillmann, J., Lupo, A. R., and Seneviratne, S.: Blocking and its response to climate change, Current climate change reports, 4, 287–300, 2018.

Yee, T. W.: Vector generalized linear and additive models: With an implementation in R, Springer, New York, USA, 2015.